Asymptotic limits of SU(2) and SU(3) Wigner functions

D.J. Rowe* H. de Guise† B.C. Sanders‡

CRM-2678

July 2000

*Department of Physics, University of Toronto, Toronto, Ontario M5S 1A7, Canada.
†Centre de Recherches Mathématiques, Université de Montréal, C.P. 6128 Succ. Centre-Ville, Montréal, Québec H3C 3J7, Canada.
‡Department of Physics, Macquarie University, Sydney, New South Wales 2109, Australia.

Abstract

Asymptotic limits are given for the SU(2) Wigner functions $\mathcal{D}^j_{mn}$ functions as $j \to \infty$ for three domains of m and n. Similar asymptotic limits are given for the SU(3) Wigner functions of an irrep with highest weight $(\lambda, 0)$ as $\lambda \to \infty$. The results are shown to be relevant to the analysis of experiments with quantum interferometers.

Résumé

On donne les limites asymptotiques des fonctions de Wigner $\mathcal{D}^j_{mn}$ de SU(2) pour $j \to \infty$ et pour trois domaines de m et n. Des limites asymptotiques similaires sont données pour les fonctions de Wigner de SU(3) d'une représentation de plus haut poids $(\lambda, 0)$ avec $\lambda \to \infty$. On montre que les résultats sont pertinents pour l'analyse d'expériences d'interférométrie.

1 Introduction

The asymptotic properties of Wigner functions provide a classical interpretation of these functions. This is of interest, for example, for the design and interpretation of quantum interferometer experiments. It is known that an optical element which linearly transforms two input modes (beams) into two output modes, is represented by a U(2) transformation [1, 2, 3, 4]. Similarly, a three-mode element is represented by a U(3) transformation[5, 6]. Typically, the input modes in multimode interferometry are minimal uncertainty wave packets containing large photon numbers [7]; as a result, the relevant U(2) and U(3) transformations are close to corresponding classical limits.

We show that different asymptotic limits correspond to different classical situations and/or to group (and Lie algebra) contractions. For example, in one limit, the group SU(2) contracts to the Euclidean group E(2) and, in another, it contracts to the Heisenberg-Weyl group HW(2) of the two-dimensional harmonic oscillator. Thus, the SU(2) Wigner functions, in the corresponding limits, approach those of E(2) and HW(2), respectively. Similar contractions apply to SU(3).

Some classical limits of the SU(2) Wigner functions are known [8, 9, 10] and have been derived by different techniques. The approach of Ref. [10], for example, uses phase-space interference methods. We consider three limits in Section II corresponding to different domains of the basis states. The results are applied, in Section III, to give corresponding limits for the SU(3) Wigner functions for an irrep of highest weight $(\lambda, 0)$.

Applications to quantum interferometers are considered briefly in the concluding section.

2 Limits of SU(2) Wigner functions

The complex extension of the su(2) Lie algebra is spanned by 2×2 complex matrices $\{J_0, J_+, J_-\}$ which satisfy the commutation relations

$$[J_0, J_\pm] = \pm J_\pm \,, \quad [J_+, J_-] = 2J_0 \,. \tag{1}$$

We consider an irrep in which these elements are represented by operators $\{\hat{J}_0, \hat{J}_+, \hat{J}_-\}$ which act, in the usual way, on a $(2j+1)$–dimensional Hilbert space spanned by vectors $\{|jm\rangle \,;\, m = -j, \ldots, +j\}$:

$$\begin{aligned} \hat{J}_0|jm\rangle &= m|jm\rangle \,, \\ \hat{J}_\pm|jm\rangle &= \sqrt{(j \mp m)(j \pm m + 1)}\; |jm \pm 1\rangle \,. \end{aligned} \tag{2}$$

Wigner functions for SU(2) are defined by

$$\mathcal{D}^j_{mn}(\alpha, \beta, \gamma) = e^{-im\alpha} d^j_{mn}(\beta) e^{-in\gamma} \,, \tag{3}$$

where

$$d^j_{mn}(\beta) = \langle jm|e^{-\mathrm{i}\beta\hat{J}_y}|jn\rangle \,, \tag{4}$$

with $\hat{J}_y = -\frac{1}{2}\mathrm{i}(\hat{J}_+ - \hat{J}_-)$, is the so-called reduced Wigner function. We consider asymptotic expressions for $d^j_{mn}(\beta)$ as $j \to \infty$, in three situations: (i) when $n \approx j$ and $m^2 \ll j^2$, (ii) when $m \approx n$ and $m^2 \approx j^2$, and (iii) when $m \approx n$ and $m^2 \ll j^2$.

2.1 Harmonic oscillator limits

For $n = j$, the reduced Wigner function, d^j_{mn}, is given by

$$d^j_{mj}(\beta) = \sqrt{\frac{(2j)!}{(j+m)!(j-m)!}}\; (\cos\beta/2)^{j+m} (\sin\beta/2)^{j-m} \,. \tag{5}$$

The derivative of this function vanishes when $\beta = \beta_m$, where β_m is the semi-classical angle for which $\cos\beta_m = m/j$. For this angle

$$\cos(\beta_m/2) = \sqrt{\frac{j+m}{2j}} \,, \quad \sin(\beta_m/2) = \sqrt{\frac{j-m}{2j}} \,, \tag{6}$$

and the substitutions

$$\beta - \beta_m = 2\phi \,, \quad j + m = s \,, \quad j - m = d \,, \tag{7}$$

give

$$\begin{aligned}(\cos\beta/2)^{j+m} &= (s/2j)^{s/2}\left[\cos\phi - \sqrt{d/s}\,\sin\phi\right]^s \\ (\sin\beta/2)^{j+m} &= (d/2j)^{d/2}\left[\cos\phi + \sqrt{s/d}\,\sin\phi\right]^d .\end{aligned} \tag{8}$$

Defining the two functions

$$X(\phi) = \cos\phi - \sqrt{\frac{d}{s}}\,\sin\phi\,, \quad Y(\phi) = \cos\phi + \sqrt{\frac{s}{d}}\,\sin\phi\,, \tag{9}$$

then gives

$$d^j_{mj}(\beta) = \sqrt{\frac{(2j)!}{s!d!}\frac{s^s d^d}{(2j)^{2j}}}\,X(\phi)^s\,Y(\phi)^d\,. \tag{10}$$

The functions $X(\phi)$ and $Y(\phi)$ satisfy

$$\frac{dX(\phi)}{d\phi} = -\sqrt{\frac{d}{s}}\,Y(\phi)\,, \quad \frac{dY(\phi)}{d\phi} = \sqrt{\frac{s}{d}}\,X(\phi)\,, \tag{11}$$

so that

$$f(\phi) = X(\phi)^s Y(\phi)^d \tag{12}$$

satisfies the equation

$$\frac{df}{d\phi} = \sqrt{sd}\,\frac{X^2 - Y^2}{XY} f\,. \tag{13}$$

For small values of ϕ,

$$\sqrt{sd}\,(X^2 - Y^2) \approx -2\sin\phi\cos\phi\,, \quad XY \approx \cos^2\phi\,. \tag{14}$$

Thus

$$\frac{df}{d\phi} \approx -4j\frac{\sin\phi}{\cos\phi} f(\phi)\,, \tag{15}$$

with solution

$$X(\phi)^s\,Y(\phi)^d \;=\; f(\phi) \approx (\cos\phi)^{4j}\,. \tag{16}$$

The asymptotic expression for the factorials when $s = j + m$ and $d = j - m$ are both large [11]

$$z! \to \sqrt{\frac{2\pi}{z}}\,e^{-z} z^{z+1}\,, \tag{17}$$

gives

$$\sqrt{\frac{(2j)!}{s!d!}\frac{s^s d^d}{(2j)^{2j}}} \to \left(\frac{j}{\pi sd}\right)^{1/4}\,. \tag{18}$$

Combining this expression with eqn. (16) gives the asymptotic expression, for large values of $j + m$ and $j - m$

$$\begin{aligned} d^j_{mj}(\beta) = (-1)^{j-m} d^j_{jm}(\beta) &\to \left(\frac{1}{\sqrt{j\,\pi}\sin\beta_m}\right)^{1/2}\left[\cos\left((\beta-\beta_m)/2\right)\right]^{4j} \\ &\to \left(\frac{1}{\sqrt{j\,\pi}\sin\beta_m}\right)^{1/2}\exp[-j(\beta-\beta_m)^2/2]\,. \end{aligned} \tag{19}$$

This asymptotic expression is compared with the exact result for a range of values of m for $j = 20$ in figure 1. It is seen to be remarkably accurate even for m close to j. It breaks down for $m = \pm j$ but then we have

$$\begin{aligned} d^j_{jj}(\beta) = [\cos(\beta/2)]^{2j} &\to \exp[-j\beta^2/4] \\ d^j_{-jj}(\beta) = [\sin(\beta/2)]^{2j} &\to \exp[-j(\beta-\pi)^2/4]\,. \end{aligned} \tag{20}$$

These results have a simple classical interpretation. A state with angular momentum j and z-component $m = j$ is a minimal uncertainty state. It has a density function $|\psi_{jj}(\theta,\varphi)|^2$ that is independent of φ and concentrated about the $\theta = 0$ direction (the z-axis). The rate of fall-off of the density with increasing angle is indicated by

$$\langle jj|e^{-i\beta\hat{J}_y}|jj\rangle = d^j_{jj}(\beta)\,, \tag{21}$$

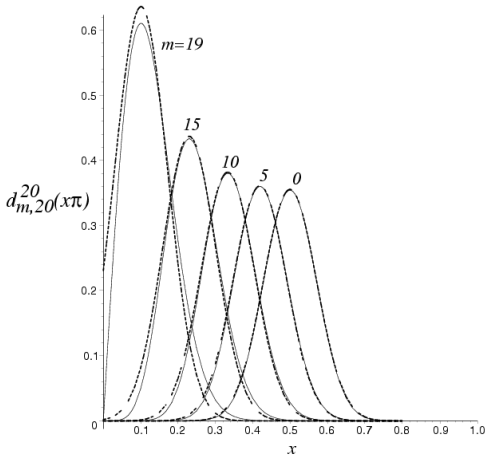

Figure 1: The reduced Wigner function $d^j_{mj}(x\pi)$ for $j = 20$ and various values of m. Exact values are shown as thin continuous lines and asymptotic values, given by eqn. (19), as broken heavy lines.

which, as seen from eqn. (20), decreases rapidly with increasing β, for large values of j. This is what one would expect from classical mechanics where the angular momentum vector is directed along the z axis when $m = j$. By the same token, a classical angular-momentum vector with z-component m makes an angle β_m with the z axis with $\cos\beta_m = m/j$. Thus, the rotated state $e^{-i\beta_m \hat{J}_y}|jj\rangle$ is expected to have maximum overlap with the state $|jm\rangle$ and conversely the overlap

$$\langle jm|e^{-i\beta \hat{J}_y}|jj\rangle = d^j_{mj}(\beta) \tag{22}$$

is expected to peak at a value of β equal to β_m, as indeed it does.

A significant property of the above asymptotic limits are that they are all simple harmonic oscillator coherent states; *i.e.,* harmonic oscillator ground state wave functions centered about β_m. We now show that, in the $j \to \infty$ limit, the other d^j_{mn} functions, for m small and $n \approx j$, approach excited harmonic oscillator coherent states.

Consider first the d^l_{0n} function, which for integer values of l, is proportional to a spherical harmonic

$$d^l_{0n}(\theta) = (-1)^n \sqrt{\frac{4\pi}{2l+1}}\, Y_{ln}(\theta, 0)\,. \tag{23}$$

For $l \to \infty$, we have, from eqn. (19), the limit

$$d^l_{0l}(\theta) \to \left(\frac{1}{\sqrt{l\pi}}\right)^{1/2} \exp[-l(\theta - \pi/2)^2/2]\,; \tag{24}$$

which is a harmonic oscillator ground-state wave function centered about $\theta = \pi/2$. Let $n = l - \nu$, so that $\nu \ll l$ when $n \approx l$. Thus, if $\psi_{l\nu}$ denotes the function

$$\psi_{l\nu}(\theta) = (-1)^\nu d^l_{0,l-\nu}(\theta + \pi/2) = (-1)^l \sqrt{\frac{4\pi}{2l+1}}\, Y_{l,l-\nu}(\theta + \pi/2, 0)\,, \tag{25}$$

then, in the $l \to \infty$ limit,

$$\psi_{l0}(\theta) \to \left(\frac{1}{\sqrt{l\pi}}\right)^{1/2} e^{-l\theta^2/2} = l^{-1/4}\, u_0(\sqrt{l}\,\theta)\,, \tag{26}$$

where u_0 is the harmonic oscillator ground-state wave function.

For $l \gg \nu$ and $l \to \infty$, the limits

$$\begin{aligned} \hat{J}_+ Y_{l,l-\nu} &= \sqrt{\nu(2l-\nu+1)}\, Y_{l,l-\nu+1} \to \sqrt{2l\nu}\, Y_{l,l-\nu+1}, \\ \hat{J}_- Y_{l,l-\nu} &= \sqrt{(2l-\nu)(\nu+1)}\, Y_{l,l-\nu-1} \to \sqrt{2l(\nu+1)}\, Y_{l,l-\nu-1}, \end{aligned} \tag{27}$$

imply that the angular momentum raising and lowering operators contract to harmonic oscillator lowering and raising operators, respectively. From the explicit expression for the actions of the $\hat{J}_\pm$ operators on spherical harmonic oscillators, we also have

$$[\hat{J}_\pm Y_{l,l-\nu}](\theta + \pi/2, 0) = \left[(l-\nu)\tan\theta \pm \frac{d}{d\theta}\right] Y_{l,l-\nu}(\theta + \pi/2, 0) \tag{28}$$

so that, for small θ and $l \gg \nu$,

$$[\hat{J}_{\pm} Y_{l,l-\nu}](\theta + \pi/2, 0) \to \left(l\theta \pm \frac{d}{d\theta} \right) Y_{l,l-\nu}(\theta + \pi/2, 0)\,. \tag{29}$$

It follows that, in the $l \to \infty$ limit,

$$\psi_{l,\nu+1}(\theta) = \frac{1}{\sqrt{2l(\nu+1)}} \left(l\theta - \frac{d}{d\theta} \right) \psi_{l\nu}(\theta) = \frac{1}{\sqrt{(\nu+1)}} \frac{1}{\sqrt{2}} \left(\sqrt{l}\,\theta - \frac{1}{\sqrt{l}} \frac{d}{d\theta} \right) \psi_{l\nu}(\theta)\,, \tag{30}$$

thereby providing a recursion relation for the $\psi_{l\nu}$ functions. Since ψ_{l0} is a harmonic oscillator ground state wave function, the recursion relation is easily solved to give

$$\psi_{l\nu}(\theta) \to l^{-1/4}\, u_{\nu}(\sqrt{l}\,\theta)\,, \tag{31}$$

where u_ν is the harmonic oscillator wave function

$$u_{\nu}(x) = \left(\frac{1}{\sqrt{\pi}\, 2^{\nu} \nu!} \right)^{1/2} H_{\nu}(x)\, e^{-x^2/2} \tag{32}$$

with H_ν a Hermite polynomial. Thus, we obtain the asymptotic limit of the Wigner function for $\nu \ll l$ and $l \to \infty$

$$d^{l}_{0,l-\nu}(\beta) \to (-1)^{\nu}\, l^{-1/4}\, u_{\nu}(\sqrt{l}\,(\beta - \pi/2))\,. \tag{33}$$

The asymptotic expression for

$$Y_{l,m}(\theta, 0) = (-1)^m \sqrt{\frac{2l+1}{4\pi}}\; d^{l}_{0,m}(\theta) \to (-1)^{l} \sqrt{\frac{2l+1}{4\pi\sqrt{l}}}\; u_{l-m}(\sqrt{l}\,(\theta - \pi/2)) \tag{34}$$

is compared with exactly computed spherical harmonics for $l = 20$ and $m = 20$, 18 and 16, in Fig. 2.

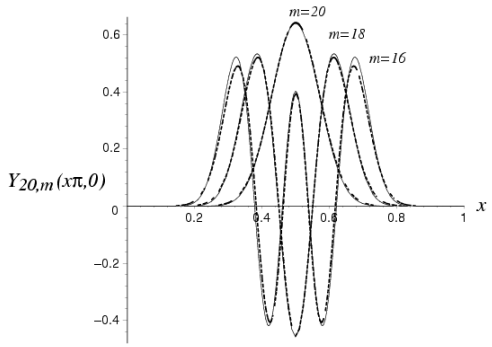

Figure 2: Spherical harmonics $Y_{20,m}(\theta, \varphi)$ for $m = 20$, 18 and 16 plotted as a function of θ for $\varphi = 0$. Exact values are shown as fine continuous lines and asymptotic values, given by eqn. (34), as heavy dashed lines.

Comparisons for $l = 20$ and $m = 19$, 17 and 15 are shown in Fig. 3.

The agreement is excellent for θ near $\pi/2$ but deteriorates as θ approaches 0 or π. This can be attributed in part to the fact that the volume element for the spherical harmonics is $\sin\theta\, d\theta$ whereas the corresponding harmonic oscillator wave functions are normalized without the factor $\sin\theta$. Thus, one expects better agreement if the asymptotic expressions are renormalized by a factor $1/\sqrt{\sin\theta}$. This indeed turns out to be the case. Fig. 4 shows that, with this adjustment, quite good agreement can be obtained even for $m = 12$.

A similar analysis can be applied to other d functions. For $l \gg \nu$ and $j \to \infty$, the equations

$$\begin{aligned} \hat{J}_{+} d^{j}_{m,j-\nu} &= \sqrt{\nu(2j-\nu+1)}\, d^{j}_{m,j-\nu+1} \to \sqrt{2j\nu}\, d^{j}_{m,j-\nu+1}, \\ \hat{J}_{-} d^{j}_{m,j-\nu} &= \sqrt{(2j-\nu)(\nu+1)}\, d^{j}_{m,j-\nu-1} \to \sqrt{2j(\nu+1)}\, d^{j}_{m,j-\nu-1}. \end{aligned} \tag{35}$$

imply that $\hat{J}_{\pm}$ can again be interpreted as a harmonic oscillator raising and lowering operators. Starting with the shifted harmonic oscillator wave functions

$$d^{j}_{mj}(\beta) \to \left(\frac{1}{\sqrt{j\pi}\, \sin\beta_m} \right)^{1/2} e^{-j(\beta-\beta_m)^2/2} = \left(\frac{1}{\sqrt{j}\, \sin\beta_m} \right)^{1/2} u_0(\sqrt{j}\,(\beta - \beta_m))\,, \tag{36}$$

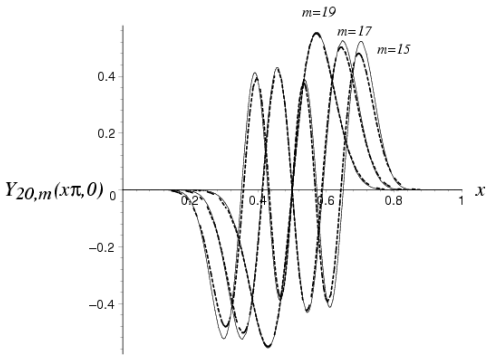

Figure 3: Spherical harmonics $Y_{20,m}(\theta,\varphi)$ for $m = 19$, 17 and 15 plotted as a function of θ for $\varphi = 0$. Exact values are shown as fine continuous lines and asymptotic values, given by eqn. (34), as heavy dashed lines.

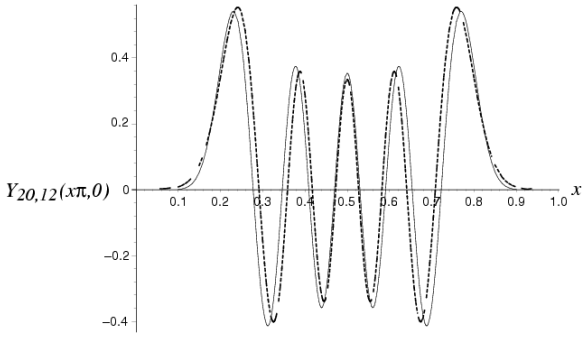

Figure 4: The spherical harmonic $Y_{20,12}(\theta,\varphi)$. Exact values are shown as a fine continuous line and asymptotic values, given by eqn. (34) multiplied by a factor $1/\sqrt{\sin\theta}$, are shown as a heavy dashed line.

we find, for small values of ν that

$$d^j_{m,j-\nu}(\beta) \to \left(\frac{1}{\sqrt{j}\sin\beta_m}\right)^{1/2} (-1)^\nu\, u_\nu(\sqrt{j}\,(\beta-\beta_m)) \tag{37}$$

as $j \to \infty$, and

$$d^j_{j-\nu,m}(\beta) \to (-1)^{j-m}\left(\frac{1}{\sqrt{j}\sin\beta_m}\right)^{1/2} u_\nu(\sqrt{j}\,(\beta-\beta_m))\,. \tag{38}$$

Fig. 5 shows the function $d^{20}_{17,3}$ compared to its asymptotic harmonic oscillator limit. Again further improvement in the limit can be obtained by dividing the asymptotic exression by $\sqrt{\sin\beta}$.

2.2 The SU(2) → HW(2) contraction

The above harmonic oscillator limits for d^j_{mn} apply when m is small and n is close to j (or vice versa) and β is close to the appropriate semi-classical angle. In practice, this means that these limits are not very good for values of β close to 0 or π. Neither are they good for $m \approx n$. In this situation, there are asymptotic limits which derive from contractions of the SU(2) Lie algebra.

We consider here a HW(2) contraction of su(2) which follows from the Holstein-Primakoff [12] representation in which the angular momenta are realized as the operators

$$\hat{J}_0 = j - \hat{n}\,, \quad \hat{J}_+ = \sqrt{2j-\hat{n}}\;a\,, \quad \hat{J}_- = a^\dagger\sqrt{2j-\hat{n}}\,; \tag{39}$$

$a^\dagger$ and a are the raising and lowering operators of a simple harmonic oscillator with commutation relation

$$[a, a^\dagger] = I\,, \tag{40}$$

and $\hat{n} = a^\dagger a$ is the number operator. In this representation, a state $|jm\rangle$ becomes a simple harmonic oscillator state $|\mu\rangle$ having $\mu = j - m$ quanta, for which $\hat{n}|\mu\rangle = \mu|\mu\rangle$. It follows that, when acting on states for which m is close to

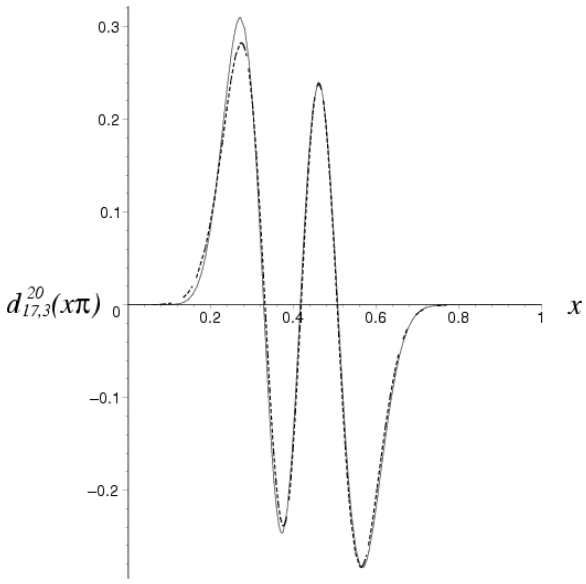

Figure 5: The Wigner function $d^{20}_{17,3}$ compared to its asymptotic harmonic oscillator limit. Exact values are shown as a fine continuous line and asymptotic values, given by eqn. (38), as a dashed line.

some value $\bar{m} \gg -j$, the angular momentum operators approach the asymptotic forms

$$\hat{J}_0 \to jI - a^\dagger a\,, \quad \hat{J}_+ \to \sqrt{j+\bar{m}}\; a\,, \quad \hat{J}_- \to \sqrt{j+\bar{m}}\; a^\dagger\,, \tag{41}$$

Likewise $\hat{J}_y \to \frac{1}{2}i\sqrt{j+\bar{m}}\,(a^\dagger - a)$ and, for m and n both close to $\bar{m} = \frac{1}{2}(m+n)$,

$$d^j_{mn}(\beta) \to \langle j-m|e^{\frac{1}{2}\beta\sqrt{j+\bar{m}}\,(a^\dagger - a)}|j-n\rangle\,. \tag{42}$$

The last expression, derived from a contraction limit of the su(2) Lie algebra, is valid for small values of β and for m and n far from $-j$. A similar expression holds for m and n far from $+j$.

From the identity

$$e^{\alpha(a^\dagger - a)} = e^{\alpha a^\dagger} e^{-\alpha^2/2} e^{-\alpha a}\,, \tag{43}$$

it follows that

$$\begin{aligned}
\langle\mu|e^{\alpha(a^\dagger - a)}|\nu\rangle &= \frac{1}{\sqrt{\mu!\nu!}}\,\langle 0|a^\mu e^{\alpha a^\dagger} e^{-\alpha a}(a^\dagger)^\nu|0\rangle e^{-\alpha^2/2} \\
&= \frac{1}{\sqrt{\mu!\nu!}}\,\langle 0|(a+\alpha)^\mu (a^\dagger - \alpha)^\nu|0\rangle e^{-\alpha^2/2} \\
&= \sqrt{\frac{\nu!}{\mu!}} \sum_p \binom{\mu}{p} \frac{(-\alpha^2)^{\nu-p}}{(\nu-p)!}\,\alpha^{\mu-\nu} e^{-\alpha^2/2}\,.
\end{aligned} \tag{44}$$

Now recall [11] that, for $\mu - \nu > -1$,

$$\sum_p \binom{\mu}{p} \frac{(-\alpha^2)^{\nu-p}}{(\nu-p)!} = L_\nu^{(\mu-\nu)}(\alpha^2)\,, \tag{45}$$

where $L_\nu^{(\mu-\nu)}$ is a generalized Laguerre polynomial. Thus, for $\mu - \nu > -1$, we obtain the identity

$$\langle\mu|e^{\alpha(a^\dagger - a)}|\nu\rangle = \sqrt{\frac{\nu!}{\mu!}}\,\alpha^{\mu-\nu}\,L_\nu^{(\mu-\nu)}(\alpha^2)\,e^{-\alpha^2/2} \tag{46}$$

and, with $\alpha = \frac{1}{2}\beta\sqrt{j+(m+n)/2}$, we obtain the asymptotic expression

$$d^j_{mn}(\beta) \to \sqrt{\frac{(j-n)!}{(j-m)!}}\,(a_{jmn}\beta)^{n-m}\,L_{j-n}^{(n-m)}(a^2_{jmn}\beta^2)\,e^{-a^2_{jmn}\beta^2/2}\,, \quad \text{for } m \le n\,, \tag{47}$$

where $a_{jmn} = \frac{1}{2}\sqrt{(2j+m+n)/2}$. This expression is valid for small values of β and $j+\bar{m} \gg n-m$. For $m \geq n$ and $j+\bar{m} \gg m-n$, the identity $d^j_{mn}(\beta) = d^j_{nm}(-\beta)$ gives

$$d^j_{mn}(\beta) \to \sqrt{\frac{(j-m)!}{(j-n)!}}\,(-a_{jmn}\beta)^{m-n}\,L^{(m-n)}_{j-m}(a^2_{jmn}\beta^2)\,e^{-a^2_{jmn}\beta^2/2}\,, \quad \text{for } m \geq n\,. \tag{48}$$

Other expressions are obtained from the symmetry properties of the d^j_{mn} functions. For example, an asymptotic expression for m close to $-j$ and n close to $+j$ is obtained from the identity

$$d^j_{mn}(\beta) = (-1)^{j-m} d^j_{-mn}(\beta+\pi)\,. \tag{49}$$

The asymptotic expression (48) is compared with the exactly computed function $d^{20}_{18,15}$ in Fig. 6. It is compared

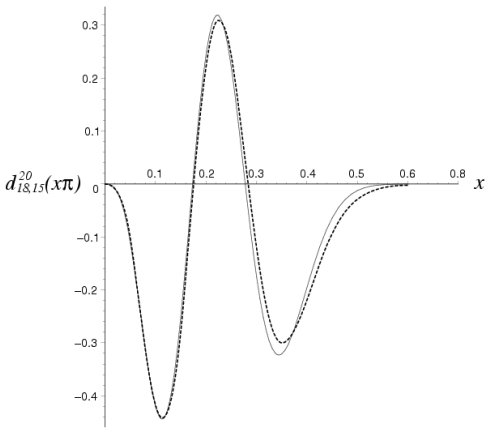

Figure 6: The reduced Wigner function $d^{20}_{18,15}(x\pi)$. Exact values are shown as a fine continuous line and asymptotic values, given by eqn. (48), as a dashed line.

with the exactly computed function $d^{20}_{6,2}$ in Fig. 7. These limits are aproached for the largest range of β when m

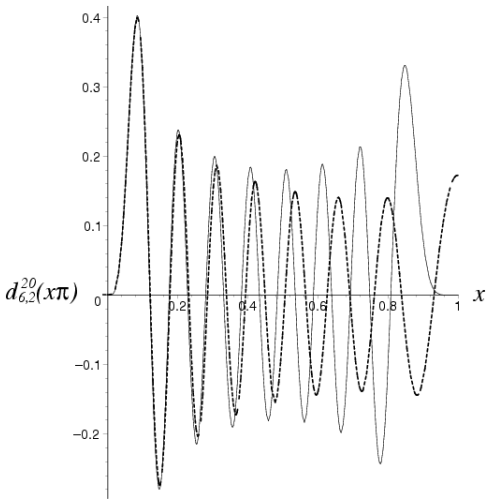

Figure 7: The reduced Wigner function $d^{20}_{6,2}(x\pi)$. Exact values are shown as a fine continuous line and asymptotic values, given by eqn. (48), as a dashed line.

and n are similar and close to $\pm j$; e.g., when d^j_{mn} is large only for $\beta < \pi/2$. This is because the su(2) $\to$ hw(2) contraction is valid to within some specified accuracy over the largest span of $\{|jm\rangle\}$ states when $|m|$ is close to j.

2.3 The SU(2) $\to$ E(2) contraction limit

For m close to n and both far from $\pm j$, a more appropriate contraction to use is the one in which SU(2) $\to$ E(2), where E(2) is the Euclidean group of transformations of the two–dimensional plane. This limit is obtained from the

observations that, as $j^2 - m^2 \to \infty$, the right hand sides of eqn. (2) approach values given by

$$\hat{J}_0|jm\rangle = m\,|jm\rangle\,,$$
$$\hat{J}_\pm|jm\rangle \to \sqrt{j^2-m^2}\,|jm\pm 1\rangle = j\sin\beta_m\,|jm\pm 1\rangle\,. \tag{50}$$

With $\cos\beta_{\bar{m}} = \bar{m}/j$, $\sqrt{j^2-\bar{m}^2} = j\sin\beta_{\bar{m}}$, and, for values of m close to $\bar{m}$, the SU(2) states are represented, in the $j^2 - \bar{m}^2 \to \infty$ limit, as functions on the circle, i.e., $|jm\rangle \to \psi_m$ with

$$\psi_m(\theta) = \frac{e^{im\theta}}{\sqrt{2\pi}}\,, \tag{51}$$

and the angular momentum operators are represented

$$\hat{J}_0 \to -\mathrm{i}\frac{d}{d\theta}\,, \quad \hat{J}_\pm \to j\sin\beta_{\bar{m}}\,e^{\pm\mathrm{i}\theta}\,. \tag{52}$$

It follows that $\hat{J}_y =\!\!\to j\sin\beta_{\bar{m}}\,\sin\theta$ and, for m and n both close to $\bar{m} = \frac{1}{2}(m+n)$,

$$d^j_{mn}(\beta) \to \frac{1}{2\pi}\int_0^{2\pi} e^{-\mathrm{i}(m-n)\theta}\,e^{-\mathrm{i}\beta j\sin\beta_{\bar{m}}\sin\theta}\,\mathrm{d}\theta = J_{n-m}(j\beta\sin\beta_{\bar{m}})\,, \tag{53}$$

where J_m is a Bessel function and we have used a known [11, 13] integral expression for J_m.

The expressions given by eqn. (52) are the limits of a general coherent state representation of the su(2) algebra carried by functions on the circle. Note, however, that since it is derived from a contraction of the Lie algebra, it is only valid locally. Thus, the asymptotic limit of eqn. (53) is only expected to be good for small values of β and $m-n$.

The asymptotic expression (53) for the reduced Wigner function $d^{20}_{6,2}$ is compared with the exact function in Fig. 8. It is seen to be an excellent approximation for small values of its argument; for $\beta < \pi/2$ it is better than the limit

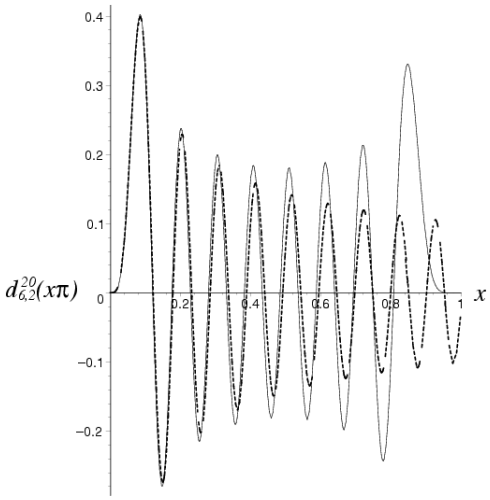

Figure 8: The reduced Wigner function $d^{20}_{6,2}(x\pi)$. Exact values are shown as a fine continuous line and asymptotic values, given by (53), as a dashed heavy line.

obtained from the SU(2) → HW(2) contraction, shown in fig. 7. This is to be expected because the E(2) limit is more appropriate for $m = 6, n = 2$ than the HW(2) limit. A much improved estimate for β in the range $\pi/2 < \beta < \pi$ is obtained by use of the identity

$$d^j_{mn}(\beta) = (-1)^{j-m}d^j_{n,-m}(\pi-\beta)\,, \tag{54}$$

which, for $\pi/2 < \beta < \pi$, leads to the asymptotic expression

$$d^j_{mn}(\beta) \to (-1)^{j-m}J_{m+n}(j(\beta-\pi)\sin\beta_{(n-m)/2})\,. \tag{55}$$

Comparison of the exact expression with the asymptotic expression (53) for β in the range $0 < \beta < \pi/2$ and with (55) for $\pi/2 < \beta < \pi$ is shown in Fig. 9. The latter result is now substantially better than the limit obtained from the SU(2) → HW(2) contraction.

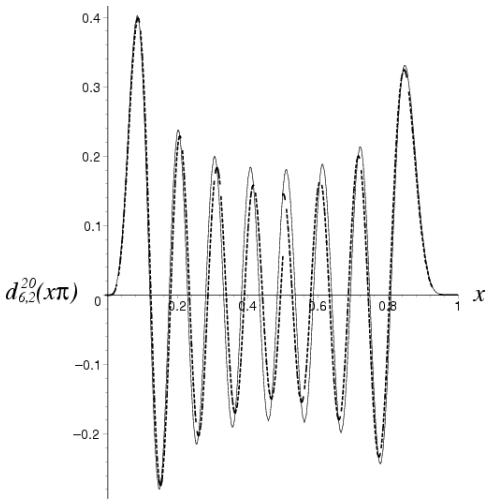

Figure 9: The reduced Wigner function $d^{20}_{6,2}(x\pi)$. Exact values are shown as a fine continuous line and asymptotic values as a dashed heavy line. For $0 < x < 0.5$ the asymptotic values are given by eqn. (53) and for $0.5 < x < 1$ they are given by eqn. (55).

For small values of β it turns out that a remarkable improvement in accuracy is obtained by the *ad hoc* replacement $j \to j + 1/2$ in the argument of the Bessel function of the asymptotic expression. This replacement has also been found by other authors to increase numerical accuracy; to first order, it can be regarded as a substitution of j by $\sqrt{j(j+1)}$, which is the appropriate classical value of the magnitude of the angular momentum. The modified estimate is compared with the exact expression for $d^{20}_{6,2}(x\pi)$ in Fig. 10.

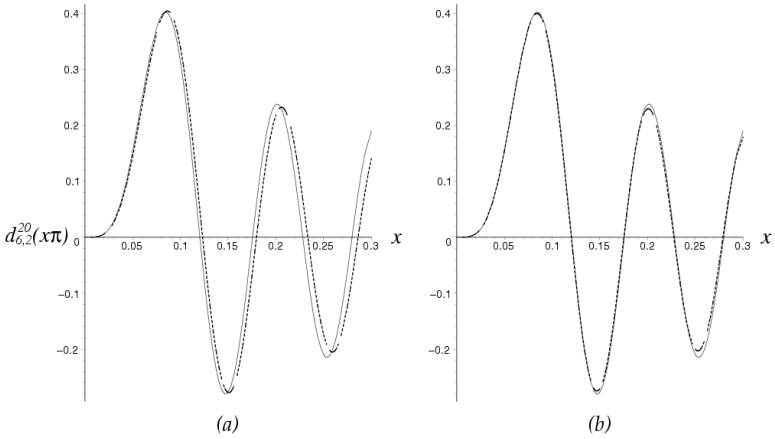

Figure 10: The reduced Wigner function $d^{20}_{6,2}(x\pi)$. Exact values are shown as a fine continuous line and asymptotic values as a dashed line. The asymptotic expression in (a) is given by eqn. (53) and in (b) it is given by (53) with j replaced by $j + 1/2$.

Fig. 11 shows a comparison of the E(2) limit of the Wigner function $d^{20}_{18,15}$, with j replaced by $j + 1/2$, with the exact function. The indices $m = 18$ and $n = 15$ are now far from the $m \approx n \approx 0$ region in which the E(2) limit is most applicable. Thus, the result is not nearly as good as that obtained from the HW(2) contraction, shown in fig. 6. Nevertheless, it is good for small values of β.

The above results have a natural interpretation in terms of an SU(2) $\to$ E(2) contraction. If we define

$$x = \frac{1}{2j \sin\beta_{\bar{m}}}(J_+ + J_-)\,, \quad y = -\frac{i}{2j \sin\beta_{\bar{m}}}(J_+ - J_-)\,, \quad J_z = J_0\,, \tag{56}$$

we obtain the commutation relations

$$[J_z, x] = \mathrm{i}y\,, \quad [J_z, y] = -\mathrm{i}x\,, \quad [x, y] = \frac{i}{j^2 \sin^2\beta_{\bar{m}}} J_z \to 0\,, \tag{57}$$

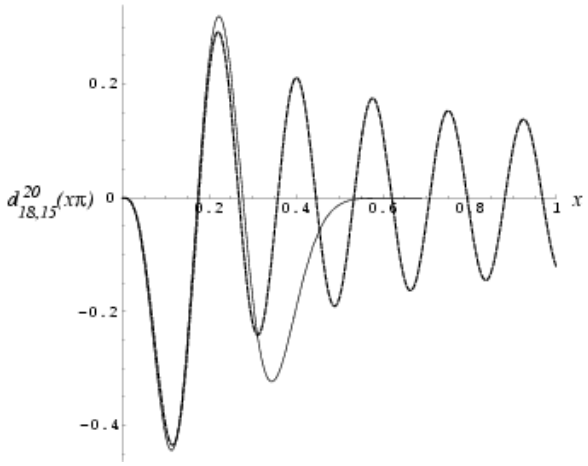

Figure 11: The reduced Wigner function $d^{20}_{18,15}(x\pi)$. Exact values are shown as a fine continuous line and asymptotic values, given by eqn. (53) with j replaced by $j+1/2$, as a dashed line.

as $j\sin\beta_{\bar{m}} \to \infty$. They are the commutations relations of the infinitesimal generators of the Euclidean group in two dimensions. Moreover, the SU(2) representation with highest weight j contracts to a representation of the Euclidean group E(2) in which

$$x \to \cos\theta\,, \quad y \to \sin\theta\,, \quad J_z \to -\mathrm{i}\frac{d}{d\theta}\,. \tag{58}$$

This contraction limit makes sense geometrically if one considers the manifold of SU(2) coherent states in the Hilbert space generated by applying all SU(2) transformations to a fixed state $|jm\rangle$. This manifold has the geometry of a sphere and one knows that small neighbourhoods on a sphere look locally like neighbourhoods of a two-dimensional Euclidean plane.

2.4 Summary of SU(2) Wigner function limits in a U(2) basis

In summarizing the limits for d^j_{mn}, it is useful to characterize the value of m as being central if $m \approx 0$ and extremal if $m \approx \pm j$. The various asymptotic limits for d^j_{mn} are then at their best in the following situations: (i) Harmonic oscillator limits; when m is central and n is extremal, (ii) HW(2) contraction limits; when m and n are both extremal, and (iii) E(2) contraction limits; when m and n are both central.

For application of the above results to SU(3), the results are most usefully expressed in a U(2) weight basis in which a state $|jm\rangle$ is identified with the U(2)-weight state $|sd\rangle$ with $s = j+m$ and $d = j-m$. A reduced SU(2) Wigner function in then expressed

$$d^j_{mn}(\beta) = \langle s_1 d_1|\beta|s_2 d_2\rangle\,, \tag{59}$$

with $s_1 = j+m$, $d_1 = j-m$, $s_2 = j+n$, and $d_2 = j-n$. The above asymptotic limits are summarized as follows.

2.4.1 Harmonic oscillator limits

If m is central then $s = j+m \gg 0$ and $d = j-m \gg 0$ in the $j \to \infty$ limit. Equations (37) and (38) are then expressed

$$\langle sd|\beta|2j-n,n\rangle = (-1)^{n-d}\langle 2j-n,n|\beta|sd\rangle \to \delta_{s+d,2j}\,(-1)^n\left(\frac{j}{sd}\right)^{\frac{1}{4}} u_n(\sqrt{j}(\beta-\beta_{sd}))\,, \tag{60}$$

where $j = (s+d)/2$ and

$$\cos\beta_{sd} = \frac{s-d}{s+d} \quad \Rightarrow \quad \sin\beta_{sd} = \frac{\sqrt{sd}}{j}\,, \tag{61}$$

and u_n is given by eqn. (32). This limit is valid for small values of n.

2.4.2 HW(2) contraction limits

If m and n are both close to j, then $s_1 \gg d_1$ and $s_2 \gg d_2$. Substituting the expression

$$a^2_{jmn} = \frac{1}{8}(2j+m+n) = \frac{1}{8}(s_1+s_2) \tag{62}$$

for a^2_{jmn} into eqns. (47) and (48) then gives, in this limit,

$$\langle s_1 d_1|\beta|s_2 d_2\rangle \to \delta_{s_1+d_1,s_2+d_2}\sqrt{\frac{d_2!}{d_1!}}\left(\frac{\beta}{2}\sqrt{\frac{s_1+s_2}{2}}\right)^{s_2-s_1} L_{d_2}^{(s_2-s_1)}(\beta^2(s_1+s_2)/8)e^{-\beta^2(s_1+s_2)/16} \tag{63}$$

for $s_1 \le s_2$ and

$$\langle s_1 d_1|\beta|s_2 d_2\rangle \to \delta_{s_1+d_1,s_2+d_2}\sqrt{\frac{d_1!}{d_2!}}\left(-\frac{\beta}{2}\sqrt{\frac{s_1+s_2}{2}}\right)^{s_1-s_2} L_{d_1}^{(s_1-s_2)}(\beta^2(s_1+s_2)/8)e^{-\beta^2(s_1+s_2)/16} \tag{64}$$

for $s_1 \ge s_2$.

If m is close to j and n is close to $-j$, so that $s_1 \gg d_1$ and $s_2 \ll d_2$, the identity $d^j_{mn}(\beta) = (-1)^{j-n}d^j_{m,-n}(\beta+\pi)$ interchanges the coefficients s_2 and d_2 to give

$$\langle s_1 d_1|\beta|s_2 d_2\rangle = (-1)^{d_2}\langle s_1 d_1|\beta+\pi|d_2 s_2\rangle \tag{65}$$

for which eqns. (63) and (64) continue to apply. Similarly, for $s_1 \ll d_1$ and $s_2 \gg d_2$,

$$\langle s_1 d_1|\beta|s_2 d_2\rangle = (-1)^{d_1}\langle d_1 s_1|\beta+\pi|s_2 d_2\rangle\,, \tag{66}$$

and, for $s_1 \ll d_1$ and $s_2 \ll d_2$, the identity $d^j_{mn}(\beta) = (-1)^{m-n}d^j_{-m,-n}(\beta)$ gives

$$\langle s_1 d_1|\beta|s_2 d_2\rangle = (-1)^{s_1-s_2}\langle d_1 s_1|\beta|d_2 s_2\rangle\,. \tag{67}$$

2.4.3 E(2) contraction limits

When m and n are both small and j is large, $s_1 \gg 0$, $d_1 \gg 0$, $s_2 \gg 0$, and $d_2 \gg 0$. Replacing $2j\sin\beta_{\bar{m}}$ by $\sqrt{(s_1+s_2)(d_1+d_2)}$ in eqn. (53) then gives

$$\langle s_1 d_1|\beta|s_2 d_2\rangle \to \delta_{s_1+d_1,s_2+d_2}J_{d_1-d_2}(\sqrt{(s_1+s_2)(d_1+d_2)}\;\beta/2)\,. \tag{68}$$

3 $(\lambda, 0)$ SU(3) Wigner functions

The complex extension of the u(3) Lie algebra is spanned by 3×3 matrices $\{C_{ij}\}$ which satisfy the commutation relations

$$[C_{ij}, C_{kl}] = \delta_{jk}C_{il} - \delta_{il}C_{kj}\,. \tag{69}$$

The su(3) $\subset$ u(3) subalgebra is spanned by the subset $\{C_{11}-C_{22}, C_{22}-C_{33}, C_{ij}; i\ne j\}$.

3.1 Representations of the u(3) Lie algebra

We consider a u(3) irrep of highest weight $(\lambda,0,0)$ in which the $\{C_{ij}\}$ matrices are represented by operators $\{\hat{C}_{ij}\}$ on a Hilbert space spanned by a weight basis $\{|\nu\rangle\}$. The components of a weight $\nu \equiv (\nu_1,\nu_2,\nu_3)$ are the eigenvalues of the $\hat{C}_{ii}$ operators, viz.

$$\hat{C}_{ii}|\nu\rangle = \nu_i|\nu\rangle\,, \quad i=1,2,3\,, \tag{70}$$

and sum to give $\nu_1+\nu_2+\nu_3 = \lambda$. For a $(\lambda,0,0)$ irrep, the weight basis states are defined uniquely, to within phase factors. Such an irrep restricts to an su(3) irrep of highest weight $(\lambda,0)$.

The basis states $\{|\nu\rangle\}$ are conveniently realized within the space of a three-dimensional harmonic oscillator. Thus, if $\{c_i^\dagger, c_i\,; i=1,2,3\}$ denotes a triplet of harmonic oscillator raising and lowering operators, the (orthonormal) weight states are

$$|\nu\rangle = \frac{(c_1^\dagger)^{\nu_1}(c_2^\dagger)^{\nu_2}(c_3^\dagger)^{\nu_3}}{\sqrt{\nu_1!\nu_2!\nu_3!}}\,|0\rangle\,, \quad \nu_1+\nu_2+\nu_3 = \lambda\,, \tag{71}$$

where $|0\rangle$ is the harmonic oscillator lowest-weight (vacuum) state, and the u(3) operators are expressed

$$\hat{C}_{ij} = a_i^\dagger a_j\,. \tag{72}$$

It follows that the $i\ne j$ operators act on the weight states according to the equation

$$\hat{C}_{ij}|\nu_1,\nu_2,\nu_3\rangle = \sqrt{(\nu_i+1)\nu_j}\;\sum_{\nu'}\delta_{\nu'_i,\nu_i+1}\delta_{\nu'_j,\nu_j-1}\delta_{\nu'_k,\nu_k}|\nu'_1,\nu'_2,\nu'_3\rangle\,, \tag{73}$$

for $i \neq k \neq j$.

The above (weight) basis reduces the $\mathrm{su}(2)_{23} \subset \mathrm{su}(3)$ subalgebra spanned by the I-spin operators

$$\hat{I}_+ = \hat{C}_{23}\,, \quad \hat{I}_- = \hat{C}_{32}\,, \quad \hat{I}_0 = \tfrac{1}{2}(\hat{C}_{22} - \hat{C}_{33})\,. \tag{74}$$

The corresponding I-spin quantum numbers are identified by setting

$$\nu_1 = \lambda - 2I\,, \quad \nu_2 = I + N\,, \quad \nu_3 = I - N\,, \tag{75}$$

and writing

$$|\nu\rangle \equiv |IN\rangle = \frac{(c_1^\dagger)^{\lambda-2I}}{\sqrt{(\lambda-2I)!}} \frac{(c_2^\dagger)^{I+N}(c_3^\dagger)^{I-N}}{\sqrt{(I+N)!(I-N)!}}|0\rangle\,. \tag{76}$$

The action of the $\mathrm{su}(2)_{23}$ operators is then expressed in the usual way by

$$\hat{I}_0|IN\rangle = N|IN\rangle\,, \quad \hat{I}_\pm|IN\rangle = \sqrt{(I \mp N)(I \pm N + 1)}\,|IN \pm 1\rangle\,. \tag{77}$$

Similarly, the $\mathrm{su}(2)_{12}$ and $\mathrm{su}(2)_{13}$ subalgebras are spanned by U-spin and V-spin operators, respectively:

$$\hat{U}_+ = \hat{C}_{12}\,, \quad \hat{U}_- = \hat{C}_{21}\,, \quad \hat{U}_0 = \tfrac{1}{2}(\hat{C}_{11} - \hat{C}_{22})\,, \tag{78}$$

$$\hat{V}_+ = \hat{C}_{13}\,, \quad \hat{V}_- = \hat{C}_{31}\,, \quad \hat{V}_0 = \tfrac{1}{2}(\hat{C}_{11} - \hat{C}_{33})\,. \tag{79}$$

Thus, we have the identifications $|\nu\rangle \equiv |IN\rangle \equiv |UM\rangle \equiv |VP\rangle$ with

$$\begin{aligned} \nu_1 &= \lambda - 2I = U + M = V + P\,, \\ \nu_2 &= I + N = U - M = \lambda - 2V\,, \\ \nu_3 &= I - N = \lambda - 2U = V - P\,. \end{aligned} \tag{80}$$

It is important to note that, for a $(\lambda, 0)$ irrep, the above weight basis becomes identical to the basis $\{|jIN\rangle\}$ constructed, for a general $\mathrm{SU}(3) \supset \mathrm{SU}(2)_{23}$ irrep, by VCS methods [14] and used in the computation of SU(3) Clebsch-Gordan coefficients [15]. (For a $(\lambda, 0)$ irrep the extra label j is redundant and can be dropped.) The bases are identified explicitly as follows. First observe that the highest weight state of the SU(3) $(\lambda, 0)$ irrep is the state

$$|\phi\rangle = \frac{(c_1^\dagger)^\lambda}{\sqrt{\lambda!}}\,|0\rangle\,. \tag{81}$$

Thus, with the observation that

$$(c_1)^{\lambda-\nu_1}(c_1^\dagger)^\lambda|0\rangle = \frac{\lambda!}{\nu_1!}(c_1^\dagger)^{\nu_1}|0\rangle\,, \tag{82}$$

we obtain the expression of the $\mathrm{U}(3) \supset \mathrm{SU}(3)$ basis states

$$|\nu\rangle = \sqrt{\frac{\nu_1!}{\lambda!\nu_2!\nu_3!}}\,(\hat{C}_{21})^{\nu_2}(\hat{C}_{31})^{\nu_3}|\phi\rangle\,. \tag{83}$$

This basis is identical to that of VCS theory,

$$|IN\rangle = \sqrt{\frac{(\lambda-2I)!}{\lambda!}}\,\frac{(\hat{C}_{21})^{I+N}(\hat{C}_{31})^{I-N}}{\sqrt{(I+N)!(I-N)!}}\,|\phi\rangle\,, \tag{84}$$

with the relationship between ν and IN given by eqn. (75). It is also identical to the Gel'fand basis $\{|\nu I\rangle\}$ used for a $(\lambda, 0)$ irrep in ref. [16] with $I = \frac{1}{2}(\nu_2 + \nu_3)$ (cf. appendix of ref. [15]).

3.2 $(\lambda, 0)$ Wigner functions for finite λ

As shown recently [16], an SU(3) element can be expressed as a product of SU(2) subgroup elements in the form

$$g(\alpha_1, \beta_1, \gamma_1, \alpha_2, \beta_2, \alpha_3, \beta_3, \gamma_3) = R_{23}(\alpha_1, \beta_1, \gamma_1)R_{12}(\alpha_2, \beta_2, \alpha_2)R_{23}(\alpha_3, \beta_3, \gamma_3)\,. \tag{85}$$

This is a particularly convenient parametrization because, in the above basis, the matrices of the $\mathrm{SU}(2)_{23}$ rotations are given by standard SU(2) Wigner functions; viz.

$$\langle I'N'|\hat{R}_{23}(\alpha, \beta, \gamma)|IN\rangle = \delta_{I'I}\mathcal{D}^I_{N'N}(\alpha, \beta, \gamma) \tag{86}$$

or, in terms of weights,

$$\langle\nu|\hat{R}_{23}(\alpha,\beta,\gamma)|\mu\rangle = \delta_{\nu_1,\mu_1}\mathcal{D}^{(\lambda-\nu_1)/2}_{(\nu_2-\nu_3)/2,(\mu_2-\mu_3)/2}(\alpha,\beta,\gamma)\,. \tag{87}$$

Similarly, for the $SU(2)_{12}$ matrix elements

$$\langle\mu|\hat{R}_{12}(\alpha,\beta,\gamma)|\mu'\rangle = \delta_{\mu_3,\mu'_3}\mathcal{D}^{(\lambda-\mu_3)/2}_{(\mu_1-\mu_2)/2,(\mu'_1-\mu'_2)/2}(\alpha,\beta,\gamma)\,. \tag{88}$$

The expressions are simplified by writing the SU(2) Wigner functions in a U(2) basis (cf. eqn. (59)) in which

$$\mathcal{D}^j_{mn}(\alpha,\beta,\gamma) = \langle j+m, j-m|\beta|j+n, j-n\rangle e^{-i(m\alpha+n\gamma)}\,. \tag{89}$$

Then

$$\begin{aligned}\langle\nu|\hat{R}_{23}(\alpha,\beta,\gamma)|\mu\rangle &= \delta_{\nu_1,\mu_1}\langle\nu_2\nu_3|\beta|\mu_2\mu_3\rangle e^{-i[(\nu_2-\nu_3)\alpha+(\mu_2-\mu_3)\gamma]/2}\,,\\ \langle\mu|\hat{R}_{12}(\alpha,\beta,\gamma)|\mu'\rangle &= \delta_{\mu_3,\mu'_3}\langle\mu_1\mu_2|\beta|\mu'_1\mu'_2\rangle e^{-i[(\mu_1-\mu_2)\alpha+(\mu'_1-\mu'_2)\gamma]/2}\,,\end{aligned} \tag{90}$$

and

$$\begin{aligned}D^{(\lambda,0)}_{\nu,\nu'}(\alpha_1,\beta_1,\gamma_1,\alpha_2,\beta_2,\alpha_3,\beta_3,\gamma_3) &= e^{-i[(\nu_2-\nu_3)\alpha_1+(\lambda-\nu_1)\gamma_1+2(\nu_1+\nu'_1-\lambda)\alpha_2+(\lambda-\nu'_1)\alpha_3+(\nu'_2-\nu'_3)\gamma_3]/2}\\ &\quad\times\sum_{n=0}^{n_{\max}} e^{in(\gamma_1-\alpha_2+\alpha_3)}\langle\nu_2\nu_3|\beta_1|\lambda-\nu_1-n,n\rangle\\ &\quad\times\langle\nu_1,\lambda-\nu_1-n|\beta_2|\nu'_1,\lambda-\nu'_1-n\rangle\langle\lambda-\nu'_1-n,n|\beta_3|\nu'_2\nu'_3\rangle\,,\end{aligned} \tag{91}$$

where $n_{\max} = \mathrm{Min}(\lambda-\nu_1,\lambda-\nu'_1)$.

Expressions for the SU(3) Wigner functions of other irreps are given in ref. [16].

4 $(\lambda,0)$ Wigner functions for $\lambda\to\infty$

Wigner functions for an SU(3) $(\lambda,0)$ irrep have a number of asymptotic expressions which can be obtained by substituting the corresponding limits for the SU(2) Wigner functions into eqn. (91). The appropriate limits depend on the location of the weights ν and ν' in the weight diagram. A weight can be characterized as extremal if it is close to a vertex, or central, if it is far from a vertex.

4.1 Limits of $(\lambda,0)$ Wigner functions for ν central and ν' close to a highest weight

When ν' is of highest weight, i.e., $\nu' = (\lambda,0,0)$, the expression for the SU(3) Wigner function of eqn. (91) reduces to

$$\begin{aligned}D^{(\lambda)}_{\nu,(\lambda)}(\alpha_1,\beta_1,\gamma_1,\alpha_2,\beta_2,\alpha_3,\beta_3,\gamma_3) &= e^{-i[(\nu_2-\nu_3)\alpha_1+(\lambda-\nu_1)\gamma_1+2\nu_1\alpha_2]/2}\\ &\quad\times\langle\nu_2\nu_3|\beta_1|\lambda-\nu_1,0\rangle\langle\nu_1,\lambda-\nu_1|\beta_2|\lambda0\rangle\,,\end{aligned} \tag{92}$$

where, to simplify the notation, we have identified the weights $(\lambda)\equiv(\lambda,0)\equiv(\lambda,0,0)$. The reduced SU(2) Wigner functions in this expression are of the type with asymptotic limits given by eqn. (19). Thus, we obtain

$$\begin{aligned}D^{(\lambda)}_{\nu,(\lambda)}(\alpha_1,\beta_1,\gamma_1,\alpha_2,\beta_2,\alpha_3,\beta_3,\gamma_3) &\to \left(\frac{\lambda}{4\,\pi^2\,\nu_1\nu_2\nu_3}\right)^{1/4} e^{-i[(\nu_2-\nu_3)\alpha_1+(\nu_2+\nu_3)\gamma_1+2\nu_1\alpha_2]/2}\\ &\quad\times e^{-[(\nu_2+\nu_3)(\beta_1-\beta_{\nu_2\nu_3})^2+\lambda(\beta_2-\beta_{\nu_1,\nu_2+\nu_3})^2]/4}\,.\end{aligned} \tag{93}$$

with $\beta_{\nu_2\nu_3}$ defined by eqn. (32).

More generally, for ν' close to the highest weight, the use of the harmonic oscillator limits of eqn. (60) give

$$\begin{aligned}&D^{(\lambda)}_{\nu,\nu'}(\alpha_1,\beta_1,\gamma_1,\alpha_2,\beta_2,\alpha_3,\beta_3,\gamma_3)\to\\ &\quad e^{-i[(\nu_2-\nu_3)\alpha_1+(\lambda-\nu_1)\gamma_1+2(\nu_1+\nu'_1-\lambda)\alpha_2+(\lambda-\nu'_1)\alpha_3+(\nu'_2-\nu'_3)\gamma_3]/2}\\ &\quad\times(-1)^{\lambda-\nu'_1}\left(\frac{\lambda-\nu_1}{4\nu_1\nu_2\nu_3}\right)^{1/4}\sum_{n=0}^{\lambda-\nu'_1} e^{in(\gamma_1-\alpha_2+\alpha_3)}\left(\frac{\lambda-n}{\lambda-\nu_1-n}\right)^{1/4}\\ &\quad\times u_n\left(\sqrt{\tfrac{1}{2}(\lambda-\nu_1)}\,(\beta_1-\beta_{\nu_2,\nu_3})\right)\,u_{2I-n}\left(\sqrt{\tfrac{1}{2}(\lambda-n)}\,(\beta_2-\beta_{\nu_1,\lambda-\nu_1-n})\right)\,d^I_{I-n,N}(\beta_3)\,,\end{aligned} \tag{94}$$

where $I=\frac{1}{2}(\nu'_2+\nu'_3)$ and $N=\frac{1}{2}(\nu'_2-\nu'_3)$. It can be seen that this expression reduces to that of eqn. (93) when $I=0$ and $\nu'=(\lambda,0,0)$.

This limiting expression for the $\lambda=60$ SU(3) Wigner function is compared with the exact expression for a range of values of its arguments in fig. 12.

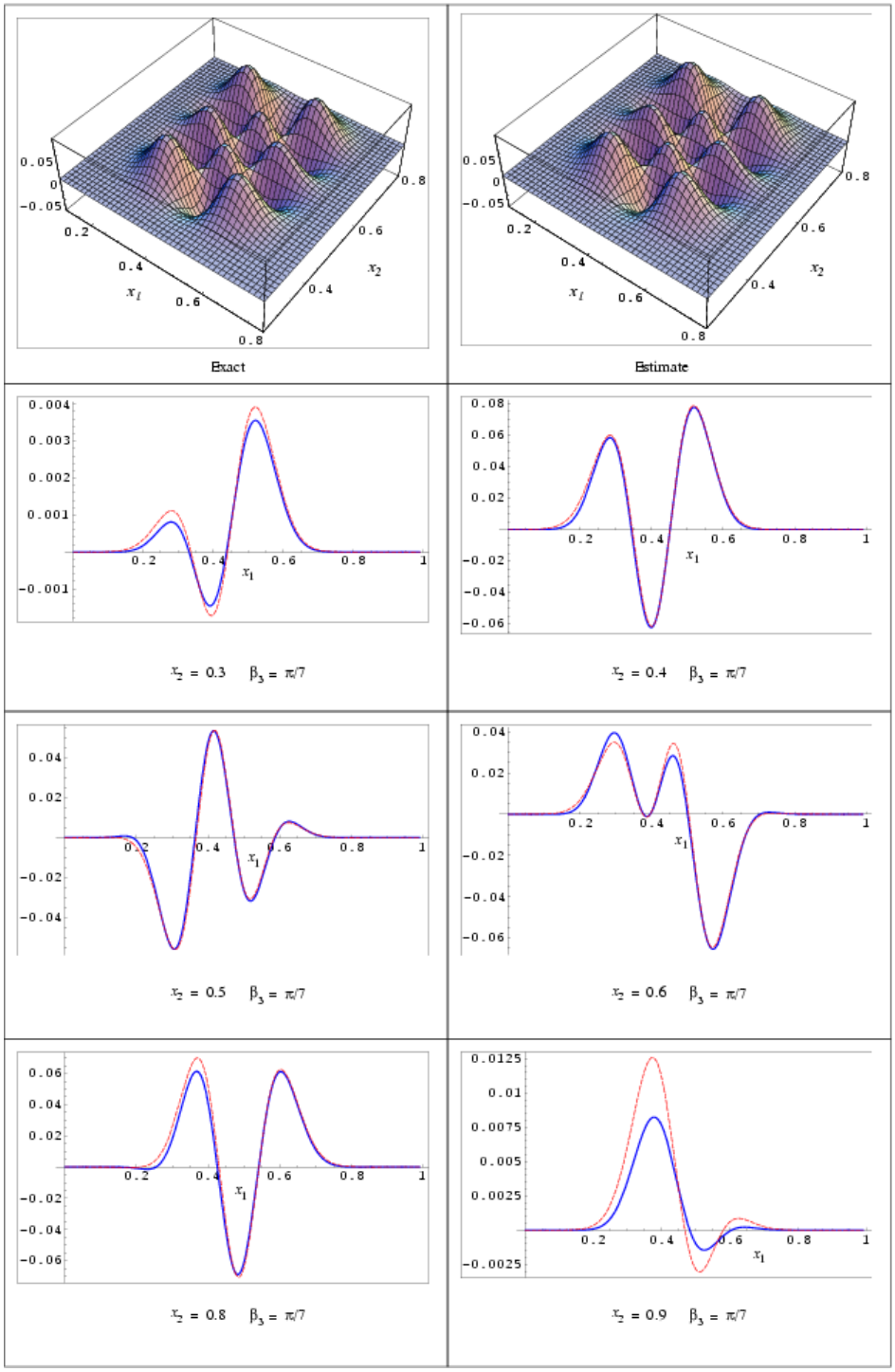

Figure 12: The SU(3) Wigner function $\mathcal{D}^{(\lambda)}_{\nu,\nu'}(0, \beta_1 = x_1\pi, 0, 0, \beta_2 = x_2\pi, 0, \beta_3 = \pi/7, 0)$ for $(\lambda) = (60, 0, 0)$, $\nu = (24, 21, 15)$, $\nu' = (54, 4, 2)$. The top graphs show, respectively, the surfaces for the exact function and its estimate using eqn. (94). The sequences of slices provide a detailed comparaison between the exact function (full line) and its estimate (dashed line) for the sequence of values of $\beta_2 = 0.3\pi$, $0.4\pi, \ldots, 0.8\pi$.

4.2 Limits of $(\lambda,0)$ Wigner functions for ν and ν' both close to vertices

If ν and ν' are both close to the highest weight, then the first and last SU(2) Wigner functions in eqn. (91) are those of small-dimensional SU(2) irreps, while, for the middle function, the limit given by eqns. (63) and (64) applies. Thus, for $\nu'_1 \geq \nu_1$,

$$\begin{aligned} D^{(\lambda)}_{\nu,\nu'}&(\alpha_1,\beta_1,\gamma_1,\alpha_2,\beta_2,\alpha_3,\beta_3,\gamma_3) \\ &\to \sum_{n=0}^{\lambda-\nu'_1} e^{-i(\nu_1+\nu'_1-\lambda+n)\alpha_2}\sqrt{\frac{(\lambda-\nu'_1-n)!}{(\lambda-\nu_1-n)!}}\left(\frac{\beta_2}{2}\sqrt{\frac{\nu_1+\nu'_1}{2}}\right)^{\nu'_1-\nu_1} \\ &\quad\times \mathcal{D}^{(\lambda-\nu_1)/2}_{(\nu_2-\nu_3)/2,(\lambda-\nu_1-2n)/2}(\alpha_1,\beta_1,\gamma_1)\,\mathcal{D}^{(\lambda-\nu'_1)/2}_{(\lambda-\nu'_1-2n)/2,(\nu'_2-\nu'_3)/2}(\alpha_3,\beta_3,\gamma_3) \\ &\quad\times L^{(\nu'_1-\nu_1)}_{\lambda-\nu'_1-n}(\beta_2^2(\nu_1+\nu'_1)/8)e^{-\beta_2^2(\nu_1+\nu'_1)/16} \end{aligned} \tag{95}$$

and, for $\nu'_1 \leq \nu_1$,

$$\begin{aligned} D^{(\lambda)}_{\nu,\nu'}&(\alpha_1,\beta_1,\gamma_1,\alpha_2,\beta_2,\alpha_3,\beta_3,\gamma_3) \\ &\to \sum_{n=0}^{\lambda-\nu_1} e^{-i(\nu_1+\nu'_1-\lambda+n)\alpha_2}\sqrt{\frac{(\lambda-\nu_1-n)!}{(\lambda-\nu'_1-n)!}}\left(-\frac{\beta_2}{2}\sqrt{\frac{\nu_1+\nu'_1}{2}}\right)^{\nu_1-\nu'_1} \\ &\quad\times \mathcal{D}^{(\lambda-\nu_1)/2}_{(\nu_2-\nu_3)/2,(\lambda-\nu_1-2n)/2}(\alpha_1,\beta_1,\gamma_1)\,\mathcal{D}^{(\lambda-\nu'_1)/2}_{(\lambda-\nu'_1-2n)/2,(\nu'_2-\nu'_3)/2}(\alpha_3,\beta_3,\gamma_3) \\ &\quad\times L^{(\nu_1-\nu'_1)}_{\lambda-\nu_1-n}(\beta_2^2(\nu_1+\nu'_1)/8)e^{-\beta_2^2(\nu_1+\nu'_1)/16}\,. \end{aligned} \tag{96}$$

This limiting expression for the $\lambda = 60$ SU(3) Wigner function is compared with the exact expression for a range of values of its arguments in fig. 13.

If ν is near $(\lambda,0,0)$ and ν' near $(0,\lambda,0)$, then the matrix element $\langle\nu_2\nu_3|\beta_1|\lambda-\nu_1-n,n\rangle$ in eqn. (91) is a reduced Wigner function for a low-dimensional SU(2) irrep. The second matrix element $\langle\nu_1,\lambda-\nu_1-n|\beta_2|\nu'_1,\lambda-\nu'_1-n\rangle$ is one for which $\nu_1 \gg \lambda-\nu_1-n$ and $\nu'_1 \ll \lambda-\nu'_1-n$. Thus, by eqn. (65), it is reexpressed in the form

$$\langle\nu_1,\lambda-\nu_1-n|\beta_2|\nu'_1,\lambda-\nu'_1-n\rangle = (-1)^{\lambda-\nu'_1-n}\langle\nu_1,\lambda-\nu_1-n|\beta_2+\pi|\lambda-\nu'_1-n,\nu'_1\rangle \tag{97}$$

for which eqns. (63) and (64) apply. The third matrix element, $\langle\lambda-\nu'_1-n,n|\beta_3|\nu'_2\nu'_3\rangle$, is one for which $\lambda-\nu'_1-n \gg n$ and $\nu'_2 \gg \nu'_3$ and for which eqns. (63) and (64) apply directly.

Asymptotic expressions are similarly found for ν and ν' near other vertices. Thus, for instance, if ν and ν' are both close to $(0,\lambda,0)$, then each of the three SU(2) Wigner functions in eqn. (91) will be approximated by the limit given by eqns. (63) or (64).

4.3 $(\lambda,0)$ Wigner functions for ν and ν' both central

If ν and ν' are both central weights of a $(\lambda,0)$ irrep and $\lambda\to\infty$, then the E(2) limit of eqn. (68) applies. If we replace the SU(2) matrix elements in eqn. (91) by their E(2) limits, we obtain

$$\begin{aligned} D^{(\lambda)}_{\nu,\nu'}(\alpha_1,\beta_1,\gamma_1,\alpha_2,\beta_2,\alpha_3,\beta_3,\gamma_3) \;\to\; & e^{-i[(\nu_2-\nu_3)\alpha_1+(\lambda-\nu_1)\gamma_1+2(\nu_1+\nu'_1-\lambda)\alpha_2+(\lambda-\nu'_1)\alpha_3+(\nu'_2-\nu'_3)\gamma_3]/2} \\ &\times\sum_{n=0}^{n_{\max}} e^{in(\gamma_1-\alpha_2+\alpha_3)}J_{\nu_3-n}(\sqrt{(2\nu_2+\nu_3-n)(\nu_3+n)}\,\beta_1/2) \\ &\times J_{\nu'_1-\nu_1}(\sqrt{(\nu_1+\nu'_1)(2\lambda-\nu_1-\nu'_1-2n)}\,\beta_2/2) \\ &\times J_{n-\nu'_3}(\sqrt{(2\nu'_2+\nu'_3-n)(\nu'_3+n)}\,\beta_3/2)\,. \end{aligned} \tag{98}$$

It is important to note that this expression presumes the E(2) limit to be applicable for all values of n that occur in the summation. The following considerations show that this presumption is valid for sufficiently small values of β_1 and β_3.

Consider the matrix element

$$\langle\nu_2\nu_3|\beta_1|\lambda-\nu_1-n,n\rangle = d^{(\lambda-\nu_1)/2}_{(\nu_2-\nu_3)/3,(\lambda-\nu_1-2n)/2}(\beta_1)\,. \tag{99}$$

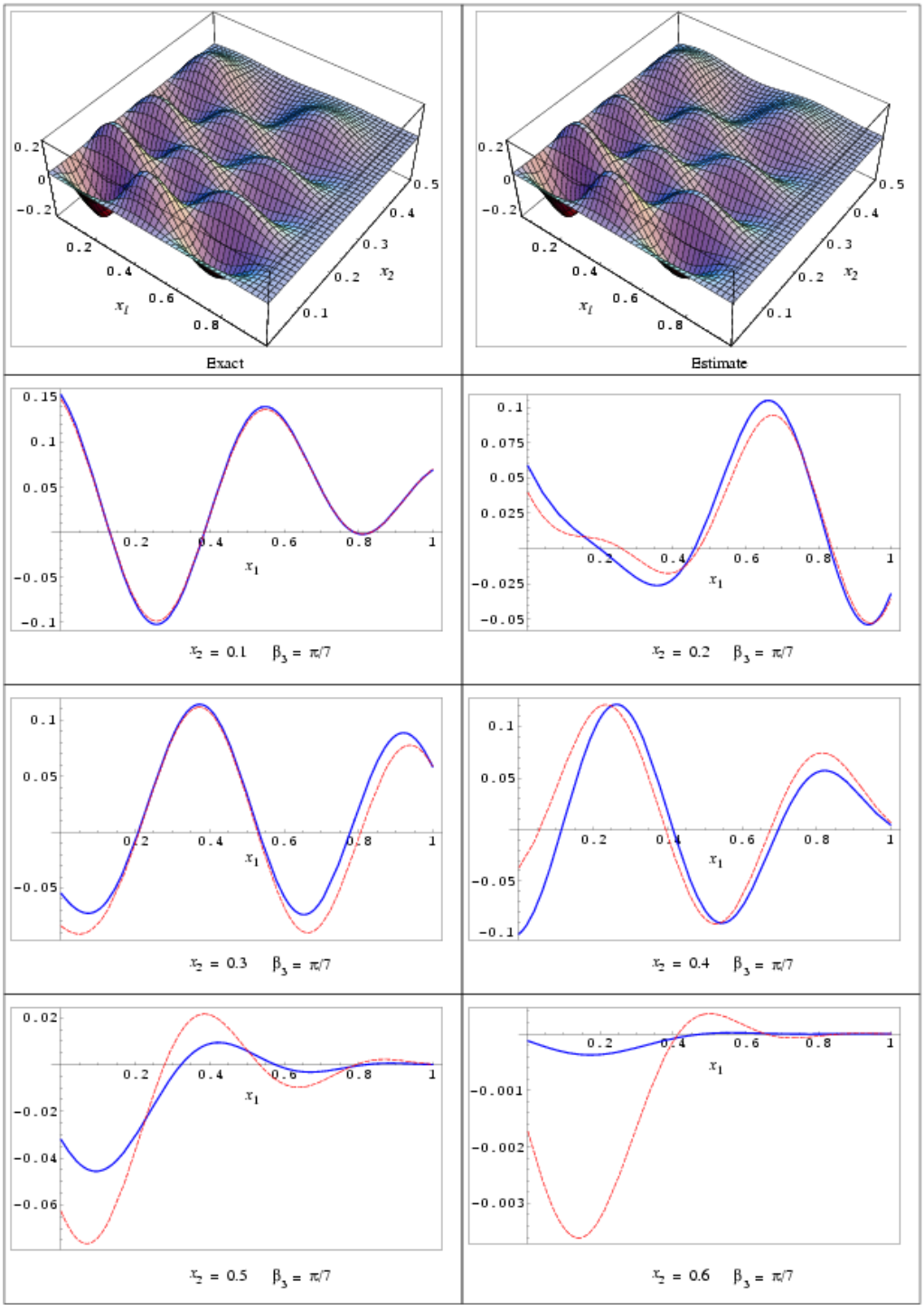

Figure 13: The SU(3) Wigner function $\mathcal{D}^{(\lambda)}_{\nu,\nu'}(0, \beta_1 = x_1\pi, 0, 0, \beta_2 = x_2\pi, 0, \beta_3 = \pi/7, 0)$ for $(\lambda) = (60, 0, 0)$, $\nu = (52, 6, 2)$, $\nu' = (50, 7, 3)$. The top graphs show, respectively, the surfaces for the exact function and its estimate using eqn. (96). The sequences of slices provide a detailed comparaison between the exact function (full line) and its estimate (dashed line) for the sequence of values of $\beta_2 = 0.1\,\pi,\ 0.2\,\pi\,, \ldots,\ 0.6\,\pi$.

For $\nu_2 = \nu_3 = \lambda/3$, for example, this matrix element becomes

$$d^{\lambda/3}_{0,\lambda/3-n}(\beta_1) = \sqrt{\frac{12\pi}{2\lambda+3}}\, Y_{\lambda/3,\lambda/3-n}(\beta_1, 0)\,. \tag{100}$$

For small β_1, it takes its largest values when $n \approx \lambda/3$. Moreover, Figs. 2 and 3 show that, for $\lambda = 60$, the value of this matrix element becomes negligible for $\beta_1 < \pi/5$ as n approaches 0. A similar result holds for the matrix element $\langle \lambda - \nu_1' - n, n|\beta_3|\nu_2'\nu_3'\rangle$ for $\nu_2' \approx \nu_3' \approx \lambda/3$.

The limiting expression (98) for the $\lambda = 150$ SU(3) Wigner function is compared with the exact expression for a range of values of its arguments in fig. 14.

5 Applications to quantum interferometry

Quantum interferometers are important in quantum information theory and for precision measurements of phases shifts, e.g., for the detection of gravitational waves [17]. The accuracies obtainable with such devices are naturally expressed in terms of Wigner functions | SU(2) Wigner functions for two–channel interferometers and SU(3) Wigner functions for three–channel interferometers.

5.1 Two-channel interferometry

A two–channel interferometer is an optical device, such as a beam splitter or a Mach-Zehnder interferometer, that transforms a two–channel input state of the electromagnetic field into a two–chanel output state. If the device consists of passive optical elements that conserve photon number (*i.e.*, the sum of the photon numbers in the output channels equals the sum in the input channels), then it is characterised by a U(2) transformation[1].

In a classical description of two–channel interferometry, the electromagnetic field is represented by a two–component complex vector $\alpha = (\alpha_1, \alpha_2)$, where α_1 and α_2 are the amplitudes of the fields in the two channels. The interferometer effects a U(2) transformation

$$\alpha^{\rm in} \to \alpha^{\rm out} = \omega\alpha^{\rm in}\,, \tag{101}$$

where

$$\omega = \begin{pmatrix} u & v \\ -v^* & u^* \end{pmatrix}, \quad \text{with } |u|^2 + |v|^2 = 1\,, \tag{102}$$

is a U(2) matrix. For example, a beam splitter effects a U(2) transformation with $u = e^{i\phi_{\rm tr}}\cos\theta$ and $v = e^{i\phi_{\rm ref}}\sin\theta$ where $\phi_{\rm tr}$ is the phase shift due to transmission, $\phi_{\rm ref}$ is the phase shift due to reflection, and $\cos\theta$ is the amplitude transmissivity of the beam splitter[2]. A lossless two–path interferometer, such as a Mach–Zehnder interferometer, is also described by a U(2) transformation; in effect a lossless two–path interferometer is equivalent to a number–conserving beam splitter.

In quantum mechanics, a closest–to–classical two–channel field is a two–component coherent state of a two–dimensional harmonic oscillator

$$|\alpha\rangle \equiv |(\alpha_1, \alpha_2)\rangle = e^{\alpha_1 a_1^\dagger - \alpha_1^* a_1} e^{\alpha_2 a_2^\dagger - \alpha_2^* a_2}|0\rangle\,, \tag{103}$$

where $|0\rangle$ is the harmonic oscillator ground state and $a_1^\dagger$ and $a_2^\dagger$ are harmonic oscillator raising operators. The raising operators transform under $\omega \in$ U(2) according to the equation

$$\begin{aligned} a_1^\dagger &\to \hat{U}(\omega) a_1^\dagger \hat{U}^\dagger(\omega) = u a_1^\dagger - v^* a_2^\dagger\,, \\ a_2^\dagger &\to \hat{U}(\omega) a_2^\dagger \hat{U}^\dagger(\omega) = u^* a_2^\dagger + v a_1^\dagger\,, \end{aligned} \tag{104}$$

from which it follows that $\hat{U}(\omega)|\alpha\rangle = |\omega\alpha\rangle$ and that the transformation of a coherent input is given by

$$|\alpha^{\rm in}\rangle \to |\alpha^{\rm out}\rangle = |\omega\alpha^{\rm in}\rangle\,. \tag{105}$$

These relationships express the correspondence between classical and quantal coherent states. More importantly, they show that an interferometer transforms any input state by a map $|\psi\rangle \to \hat{U}(\omega)|\psi\rangle$. An arbitrary input state $|\psi\rangle$ is a superposition $\sum_{jm} c_{jm}|jm\rangle$ of basis states defined in a Schwinger representation by

$$|jm\rangle = \frac{(a_1^\dagger)^{j+m}(a_2^\dagger)^{j-m}}{\sqrt{(j+m)!(j-m)!}}\,|0\rangle\,, \quad m = -j, \ldots + j\,. \tag{106}$$

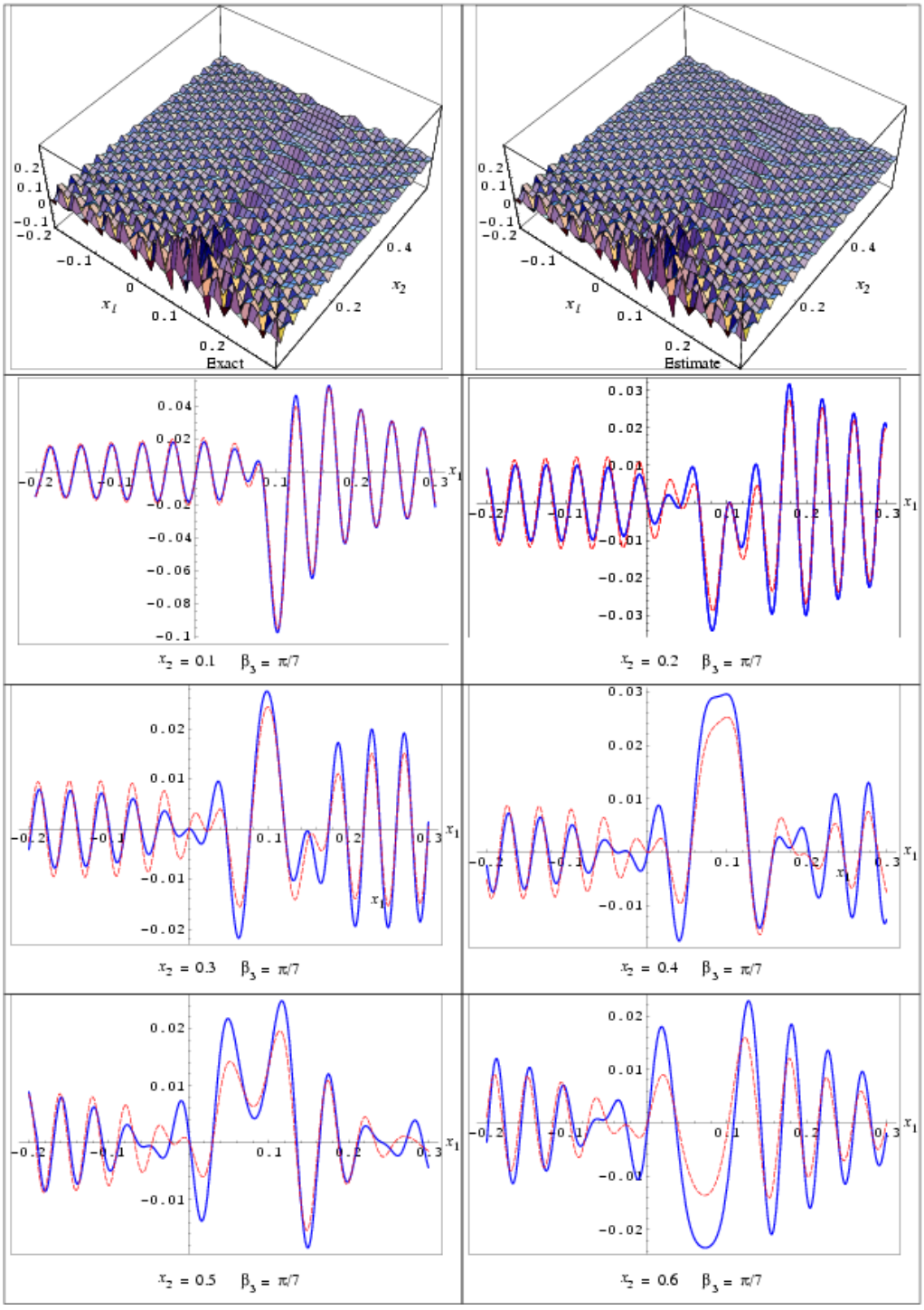

Figure 14: The SU(3) Wigner function $\mathcal{D}^{(\lambda)}_{\nu,\nu'}(0, \beta_1 = x_1\pi, 0, 0, \beta_2 = x_2\pi, 0, \beta_3 = -\pi/9, 0)$ for $(\lambda) = (150, 0, 0)$, $\nu = (46, 44, 49)$, $\nu' = (47, 52, 51)$. The top graphs show, respectively, the surfaces for the exact function and its estimate using eqn. (98). The sequences of slices provide a detailed comparison between the exact function (full line) and its estimate (dashed line) for the sequence of values of $\beta_2 = 0.1\,\pi, 0.2\,\pi, \ldots, 0.6\,\pi$.

Such states are identified with fields having a fixed number, $2j$, of photons; an input state $|jm\rangle$ is one with $j+m$ photons in channel one and $j-m$ in channel two. Thus the transformation of an arbitrary state is expressed in terms of SU(2) Wigner functions

$$\hat{U}(\omega) \;:\; |\psi\rangle \to |\psi'\rangle = \hat{U}(\omega)|\psi\rangle = \sum_{jmn} c_{jm}\,|jn\rangle\,\mathcal{D}^{j}_{nm}(\omega)\,, \quad \omega \in \mathrm{SU}(2)\,. \tag{107}$$

It is interesting to note that a minimal uncertainty state entering channel one

$$|(\alpha,0)\rangle = e^{\alpha a_1^\dagger - \alpha^* a_1}|0\rangle\,, \tag{108}$$

is a coherent state of the Heisenberg–Weyl group, whereas the state

$$\hat{U}(\omega)|jm{=}j\rangle \tag{109}$$

is a coherent state of the group U(2), according to the generalized definition of coherent states by Perelomov and others [18]. Thus a state emerging from a quantum inteferometer when the input is the state $|(\alpha,0)\rangle$ is a combined Heisenberg–Weyl – U(2) coherent state

$$|\omega(\alpha,0)\rangle = \hat{U}(\omega)e^{\alpha a_1^\dagger - \alpha^* a_1}|0\rangle\,. \tag{110}$$

Some of the interesting questions in quantum interferometry concern the measurement of phase shifts of specially prepared quantum input states. Consider, for example, the phase shift

$$\alpha_1 \to e^{-i\theta}\alpha_1\,, \quad \alpha_2 \to \alpha_2\,, \tag{111}$$

of a classical input. With the understanding that only relative phase shifts of the two components (α_1,α_2) are measured, such a phase shift is equivalent to

$$\alpha_1 \to e^{-i\theta/2}\alpha_1\,, \quad \alpha_2 \to e^{i\theta/2}\alpha_2\,. \tag{112}$$

Thus the equivalent transformations of quantum mechanical states are generated by

$$a_1^\dagger \to e^{-i\theta/2}a_1^\dagger\,, \quad a_2^\dagger \to e^{i\theta/2}a_2^\dagger\,. \tag{113}$$

It is then seen that the corresponding transformation $|jm\rangle \to e^{-im\theta}|jm\rangle$ of an SU(2) weight state is an overall phase change and undetectable. However, the transformation becomes detectable in a symmetric quantum interferometer in which the beams pass through beam splitters immediately before and immediately after they are phase shifted. If the first beam splitter effects an SU(2) transformation $e^{-i\hat{J}_x\pi/2}$ and the second reverses the transformation of the first, then the net result of the quantum interferometer is a detectable transformation in which

$$|jm\rangle \to e^{i\hat{J}_x\pi/2}e^{-i\theta\hat{J}_z}e^{-i\hat{J}_x\pi/2}|jm\rangle = e^{-i\theta\hat{J}_y}|jm\rangle = \sum_n |jn\rangle\,d^{j}_{nm}(\theta)\,. \tag{114}$$

In such an interferometer, a minimal uncertainty input $|(\alpha,0)\rangle$ is transformed to an ouput $|(\alpha\cos(\theta/2),\alpha\sin(\theta/2))\rangle$. Thus, the ratio $\tan(\theta/2)$ of the output amplitudes provides a measure of θ; if only intensities are measured it provides a measure of θ modulo π. Measurements of phase shifts can also be made with other input states and it is of interest to consider choices with the greatest potential for accuracy.

The potential accuracy of a phase shift measurement is given by the width of the distribution function

$$N_\theta(\varphi) = |\langle\psi(\theta)|e^{-i\varphi\hat{J}_y}|\psi\rangle|^2 = |\langle\psi|e^{-i(\varphi-\theta)\hat{J}_y}|\psi\rangle|^2\,. \tag{115}$$

It follows that $N_\theta(\varphi) = P(\varphi-\theta)$ where

$$P(\theta) = |\langle\psi|e^{-\theta\hat{J}_y}|\psi\rangle|^2\,. \tag{116}$$

For example, if $|\psi\rangle$ is the highest weight state $|jm{=}j\rangle$ then $P(\theta)$ is given by eqn. (20),

$$P_1(\theta) = |d^{j}_{jj}(\theta)|^2 = \exp[-j\theta^2/2]\,. \tag{117}$$

On the other hand, if $|\psi\rangle$ is the state $|j\,m{=}0\rangle$, then $P(\theta)$ has the asympotic expression given by eqn. (53),

$$P_2(\theta) = |d^{j}_{00}(\theta)|^2 \sim |J_0(j\theta)|^2\,. \tag{118}$$

Thus, in spite of the fact that the highest weight state $|jj\rangle$ is a minimal uncertainty state, the variance in θ when the input state is $|jj\rangle$ is proportional to $1/\sqrt{j}$, whereas for a $|j\,m=0\rangle$ input state, it is proportional to $1/j$. This can be understood as follows. The density distribution of a spherical harmonic $|Y_{jj}(\theta,\varphi)|^2$ is concentrated about the $\theta = 0$ pole whereas the density $|Y_{j0}(\theta,\varphi)|^2$ is spread uniformly about the $\theta = \pi/2$ equatorial circumference. Thus, the variance in θ can be much smaller for the latter distribution without violation of the uncertainty principle. This raises the question as to whether or not there might exist states with even less uncertainty relative to the $\hat{J}_y$ orientation than the state $|j0\rangle$. One candidate is the so–called SU(2) phase states[3, 6, 19]

$$|j\varphi\rangle = (2j+1)^{-1/2}\sum_{\mu=-j}^{j} e^{i\mu\varphi}|y;j\mu\rangle\,, \tag{119}$$

where $|y;j\mu\rangle$ is an eigenstate of $\hat{J}_y$ with eigenvalue μ. Putting $|\psi\rangle$ equal to $|j\varphi\rangle$ in eqn. (116) gives

$$P_3(\theta) = |\langle j\varphi|e^{-i\theta\hat{J}_y}|j\varphi\rangle|^2 = (2j+1)^{-2}\Big|\sum_{\mu} e^{i\mu\theta}\Big|^2 = (2j+1)^{-2}|\chi_j(\theta)|^2\,, \tag{120}$$

where χ_j is the well-known character of the SU(2) irrep of angular momentum j. Thus,

$$P_3(\theta) = \frac{\sin^2[(2j+1)\theta/2]}{(2j+1)^2\sin^2[\theta/2]}\,. \tag{121}$$

The function P_3 is also familiar in diffraction theory. The variance of φ for this function is proportional to $1/(j+0.5)$.

The distribution function $P(\theta)$ is shown in fig. 15 for each of the three inputs states $|jj\rangle$, $|j0\rangle$, and $|j\theta\rangle$. The figure shows that the phase state and the $m = 0$ state give much more accurate measurements than the highest weight state. The down side is that these states are much more difficult to prepare and measure than a coherent mixture of $m = j$ minimal uncertainty states. (Another candidate for improving the estimation of phase is the so-called intelligent state[20], which is also difficult to prepare.)

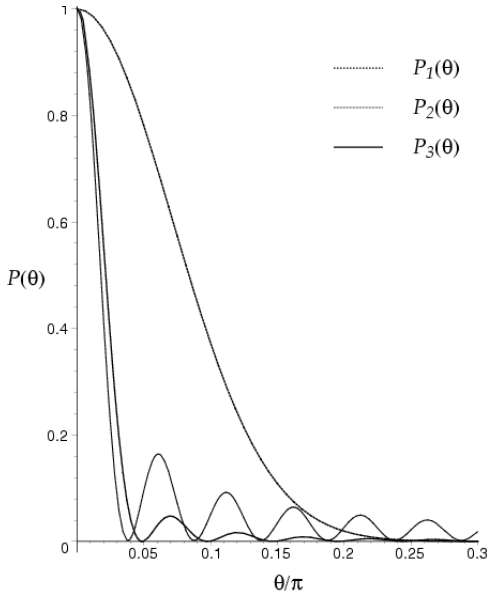

Figure 15: The distribution functions given by eqns. (117), (118), and (121) for $j = 20$.

The advantage of using $|j\,m=0\rangle$ or SU(2) phase states over $|j\,m=j\rangle$ states for precision measurements is an example of the greater potential for acquiring or transmitting information by quantal states than is possible with classical states. A highest weight state $|jj\rangle$ is a state with all photons in channel one. A classical–like coherent state

$$|(\alpha,0)\rangle = e^{\alpha a_1^\dagger - \alpha^* a_1}|0\rangle\,, \tag{122}$$

is a superposition of many highest weight states:

$$|(\alpha,0)\rangle = e^{-|\alpha|^2/2}\sum_j \frac{\alpha^{2j}}{\sqrt{(2j)!}}|jj\rangle\,. \tag{123}$$

The distribution function for a coherent state is given by

$$\left|\left\langle (\alpha,0)\left|e^{-i\theta\hat{J}_y}\right|(\alpha,0)\right\rangle\right|^2 = |\langle(\alpha,0)|(\alpha\cos(\theta/2),\alpha\sin(\theta/2))\rangle|^2 = e^{-|\alpha|^2(1-\cos(\theta/2))}\,. \tag{124}$$

Thus, if $|\alpha|^2$ is set equal to the average number of photons, $2j$, then as $j\to\infty$ this distribution function approaches the value $\exp[-j\theta^2/2]$ that it has for the number state $|jj\rangle$ as one would expect.

In contrast, the state $|j\,m{=}0\rangle$ is unlike any classical state. In quantum mechanics it is a state

$$|j0\rangle = \frac{(a_1^\dagger)^j(a_2^\dagger)^j}{j!}|0\rangle\,, \tag{125}$$

having an equal number of photons in each channel. Whereas the preparation of such a state has not been performed, a compromise state is the coherent linear superposition of such states given [21] by a two–mode squeezed coherent state

$$e^{\beta(a_1^\dagger a_2^\dagger - a_1 a_2)}|0\rangle = \mathrm{sech}\beta\sum_{j=0}^{\infty}(\tanh\beta)^j\,|j\,m{=}0\rangle\ . \tag{126}$$

This state produces the desired $1/\langle j\rangle$ scaling of the phase uncertainty[22] for the appropriately weighted average value of j. However, apart from the problems of producing such a squeezed state, it is also noted that the distribution of j values is heavily weighted in favour of low–j values. Thus, it is doubtful that much could be gained by the use of such squeezed states[3].

One might suppose that a classical–like input

$$|(\alpha,\alpha)\rangle = e^{\alpha a_1^\dagger - \alpha^* a_1}e^{\alpha a_2^\dagger - \alpha^* a_2}|0\rangle\,, \tag{127}$$

with equal amplitudes in each of the two ports might have some advantages. Such a state corresponds to an equal distribution of photon numbers in each port with a relatively narrow spread about some mean value. However, it follows from eqn. (105) that

$$|(\alpha,\alpha)\rangle = e^{-i\hat{J}_y\pi/2}\,|(\sqrt{2}\,\alpha,0)\rangle\,. \tag{128}$$

Hence

$$P(\theta) = |\langle(\alpha,\alpha)|e^{-i\theta\hat{J}_y}|(\alpha,\alpha)\rangle|^2 = |\langle(\sqrt{2}\,\alpha,0)|e^{-i\theta\hat{J}_y}|(\sqrt{2}\,\alpha,0)\rangle|^2\,, \tag{129}$$

and the variance is precisely the same as for the input state $|(\sqrt{2}\,\alpha,0)\rangle$. It should be noted that, whereas the state $|(\alpha,\alpha)\rangle$ can be obtained by an SU(2) rotation of the state $|(\sqrt{2}\,\alpha,0)\rangle$, it is impossible to rotate a highest weight state $|jj\rangle$ into the state $|jm{=}0\rangle$.

The optimization of the inputs to an interferometer in order to yield the most precise phase shift information possible with a limited number of photons is important; e.g., for the detection of gravitional waves [17]. Caves has suggested injecting a standard coherent state into one channel and a squeezed vacuum state into the other. Another suggestion is to put a squeezed input into one channel and an antisqueezed input into the other [23]. Clearly an expansion of such inputs in an SU(2) basis will make it possible to analyse the precisions obtainable with such inputs in the large photon number limit using the asymptotic SU(2) Wigner functions given in this paper.

5.2 Three–channel interferometry

Similar considerations apply to a three–channel interferometer which transforms input states by a U(3) transformation

$$T(g)\ :\ |\psi\rangle \to T(g)|\psi\rangle\,,\quad g\in \mathrm{U}(3)\,. \tag{130}$$

The transformation is analogous to the U(2) transformation discussed in the previous section, but with $T(g)$ a unitary representation of a matrix $g\in$ U(3). The U(3) transformation can be factorized into a sequence of SU(2) transformations and an overall phase factor; physically, this corresponds to a realization of a three–channel interferometer as a combination of two–channel devices (phase shifters, mirrors and beam splitters).

The infinitesimal generators of the unitary transformation $T(g)$ are given in a generalized Schwinger representation in Eqn.(72). In such a representation, basis states for an SU(3) irrep of highest weight $(\lambda,0)$ are weight states $|\nu\rangle \equiv |\nu_1\nu_2\nu_3\rangle$; they can be regarded as triplet Fock number states with ν_i photons in channel i of the interferometer and fixed total photon number.

Many of the results for two–channel interferometry, discussed in the previous section, carry forward to the three–channel case in an intuitively clear manner. For instance, the state in which all photons enter through channel one is the minimal uncertainty (highest weight) state $|(\lambda)\rangle \equiv |\lambda,0,0\rangle$. For analysis of experiments with such an input state,

the SU(3) Wigner function $D^{(\lambda)}_{\nu,(\lambda)}$ and its asymptotic limit is relevant. On the other hand, the Wigner functions for central weights are relevant for balanced input states.

Whereas the two–channel interferometer is suited to the measurement of phase difference between two channels of propagation, it may be desirable to measure multiple phase shifts simultaneously, e.g., because the phase shifts are transient or the mean particle flux of the source is limited. Moreover, the most efficient use of photons for precision measurement is to divide them up and measure relative phases between multiple paths [7, 6]. The SU(N) interferometer is ideally suited for this purpose. The SU(3) interferometer allows the measurement of two phase shifts simultaneously.

D'Ariano and Paris[7] have shown that much improved accuracy is already obtained with an easily produced coherent state input by suitably dividing the input into the many channels of a multichannel interferometer. They show that with a mean number λ of photons, the variance of the phase shift estimation scales as $\Delta\theta^2 \propto 1/N^2\lambda$ for an N-channel interferometer. In contrast, if the fixed input of λ photons were to be split between $N-1$ two–channel interferometers, then the variance of each would be proportional to $(N-1)/\lambda$ and, with the estimate of θ given by the mean of the θ_i obtained in the two–channel interferometers, the variance would be independent of N (assuming the spread of measured phase shifts is small compared to the range 0 to 2π). Thus, nothing is gained by splitting the λ photons over many two–channel interferometers but a huge gain results from appropriate use of a multichanned interferometer.

Still further gains can, in principle, be achieved by use both of exotic inputs and multichannel interferometers. The balanced input state is a preferred input state for phase–shift determination but it is hard to generate. Also, it is just one of many inputs which can, in principle, improve the precision of phase–shift estimation. The generalization to SU(3) of the SU(2) phase state considered in the previous section [6], could also yield superior scaling laws for the phase–shift estimation in terms of λ. The precision of two simultaneously measured phase shifts is rigorously expressed in terms of the covariance matrix for the two phases. This 2×2 matrix includes the variance for each phase and the covariance between the two phases. Detailed analyses of the results achievable with various techniques and three–channel inputs is in principle possible by expanding the inputs in an SU(3) basis and using the asymptotic Wigner functions to infer variances as done for two–channel interferometers in section V A.

6 Concluding remarks

In this paper, we have extended some previously known asymptotic limits of SU(2) Wigner functions and introduced new limits. We have also shown how SU(3) Wigner functions for multiplicity–free irreps of highest weight $(\lambda, 0)$ can be factored into products of SU(2) Wigner functions so that their limits can be inferred from those of SU(2). This kind of inference is not limited to SU(3) and can be generalized to SU(N) irreps of highest weight $(\lambda, 0, \ldots)$ for $N > 3$.

Explicit limiting expressions have been given for some representative classes of SU(3) Wigner functions. In particular, we have considered Wigner functions for states whose weights are either extremal or central in the terminology of sect. IV. Other expressions can be derived by variations of the methods given. For example, useful asymptotic SU(3) Wigner functions can be determined for which one weight is extremal and the other is close to a side. Depending on the domains of the initial and final states of a Wigner function, it will often happen that the expressions are much simpler in some other set of SU(3) Euler angles than those given. This is a simple reflection of the fact that a given SU(3) transformation may be simple when expressed as one sequence of SU(2) transformations but seemingly complex when expressed in some other way. Thus, by choosing the most appropriate sequence the number of summations over products of SU(2) Wigner functions can be minimized.

Asymptotic limits of Wigner functions are of interest for many reasons. In situations where they are valid, they can facilitate computations and provide quick estimates of the behaviours of quantum systems. In this way they give physical insight into the ways quantal systems approach classical limits. This has been illustrated in this paper by using the limits to estimate variances in phase shift measurements by quantum interferometry and to determine they ways they scale with the number of photons. Asymptotic limits may also be important in quantum information theory for identifying quantum states that behave in very non–classical and potentially useful ways.

References

[1] B. Yurke, S.L. McCall and J.R. Klauder, Phys. Rev. A **33**, 4033 (1986).

[2] R. A. Campos, B. E. A. Saleh and M. C. Teich, Phys. Rev. A **40**, 1371 (1989).

[3] B.C. Sanders and G.J. Milburn, Phys. Rev. Lett. **75**, 2944 (1995); B.C. Sanders, G.J. Milburn and Z. Zhang, J. Mod. Optics **44**, 1309 (1997).

[4] R. Walser, Phys. Rev. Lett. **79**, 4724 (1997).

[5] M. Reck, A. Zeilinger, H.J. Bernstein and P. Bertani, Phys. Rev. Lett. **73**, 58 (1994).

[6] B. C. Sanders, H. de Guise, D. J. Rowe and A. Mann, J. Phys. A: Math. Gen., **32**, 7791 (1999).

[7] G, D'Ariano and M. G. A. Paris, Phys. Rev. A **55**, 2267 (1997).

[8] D. A. Varshalovich, A.N. Moskalev, and V.K. Khersonskii, "Quantum theory of angular momentum" (World Scientific, Singapore, 1988) p. 115.

[9] P. J. Brussaard and H.A. Tolhoek, Physics **23**, 955 (1957).

[10] C. C. Lassig and G. J. Milburn, Phys. Rev. A **48**, 1854 (1993).

[11] *Handbook of Mathematical Functions*, ed. M. Abramowitz and I. Stegun (Dover, New York, 1965.

[12] T. Holstein and H. Primakoff, Phys. Rev. **58**, 1098 (1940).

[13] W. Magnus, F. Oberhettinger and R.P. Soni, *Formulas and Theorems for the Special Functions of Mathematical Physics* (Springer-Verlag, 1966)

[14] D. J. Rowe and J. Repka, J. Math. Phys. **38**, 4363 (1997).

[15] D. J. Rowe and C. Bahri, *The matrices and coupling coefficients of SU(3)*, Univ. of Toronto preprint.

[16] D. J. Rowe, B. C. Sanders and H. de Guise, J. Math. Phys. **40**, 3604 (1999).

[17] C. M. Caves, Phys. Rev. D **23**, 1693 (1981).

[18] A. Perelomov, Commun. Math. Phys. **26** 222, (1972); "Generalized Coherent States and their Applications," Springer, Berlin, 1986; R. Gilmore, Ann. Phys. (N.Y.) **74**, 391, (1972); J. R. Klauder, J. Math. Phys. **4**, 1058 (1963); J. R. Klauder and B-S. Skagerstam, "Coherent States" (World Scientific, Singapore 1985).

[19] A. Vourdas, Phys. Rev. A **41**, 1653 (1990).

[20] C. Brif and A. Mann, Phys. Rev. A **54**, 4505 (1996).

[21] C. M. Caves and B. L. Schumaker, Phys. Rev. A **31**, 3068 (1985); B. L. Schumaker and C. M. Caves, Phys. Rev. A **31**, 3093 (1985)

[22] M. J. Holland and K. Burnett, Phys. Rev. Lett. **71**, 1355 (1993).

[23] P. Grangier, R. E. Slusher, B. Yurke and A. LaPorta, Phys. Rev. Lett. **59**, 2153 (1987).